JHC ex*PRESS*
Accepted for publication on April 23, 2008
This article may be cited as DOI: 10.1369/jhc.2008.950543

Figure 6

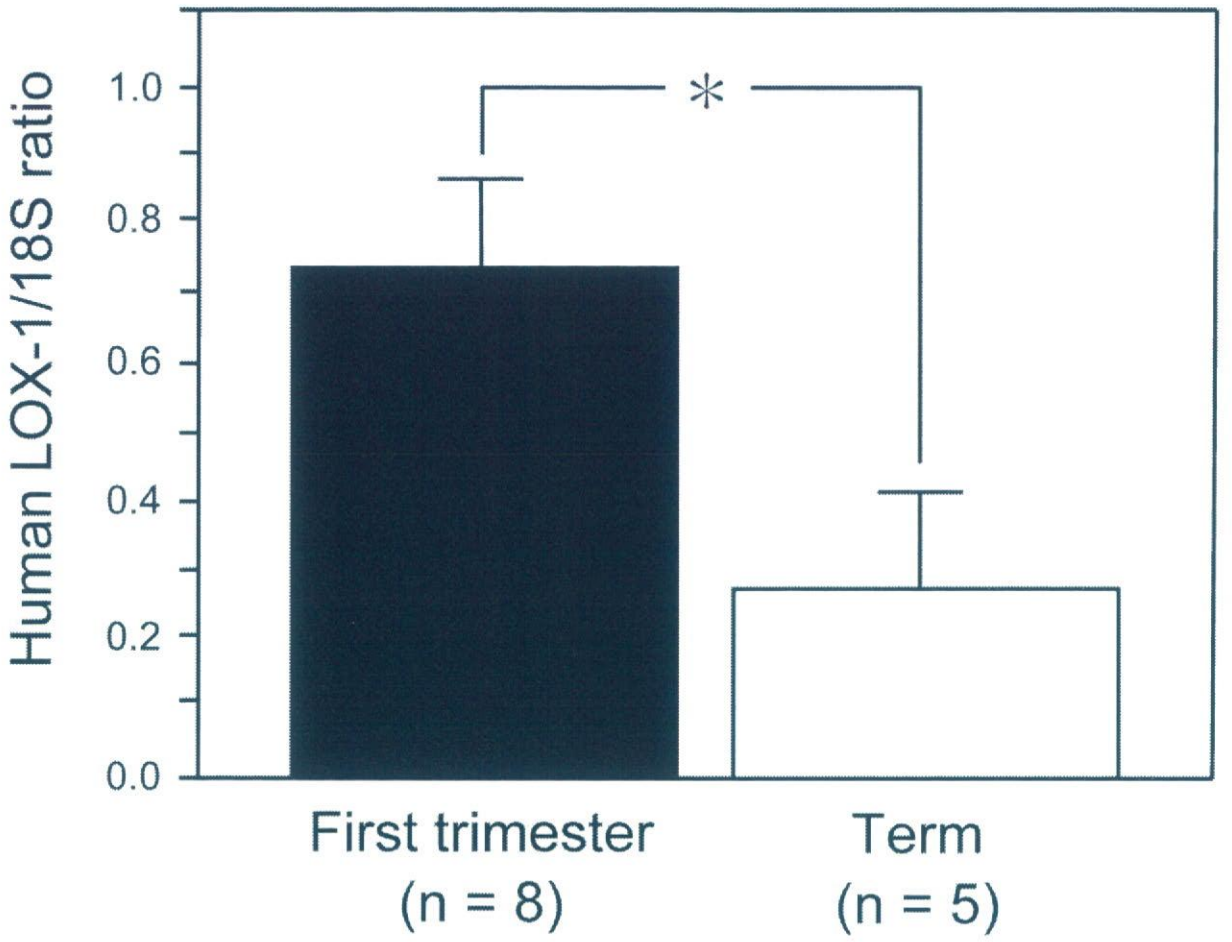

JHC ex*PRESS*
Accepted for publication on April 23, 2008
This article may be cited as DOI: 10.1369/jhc.2008.950543

Figure 7

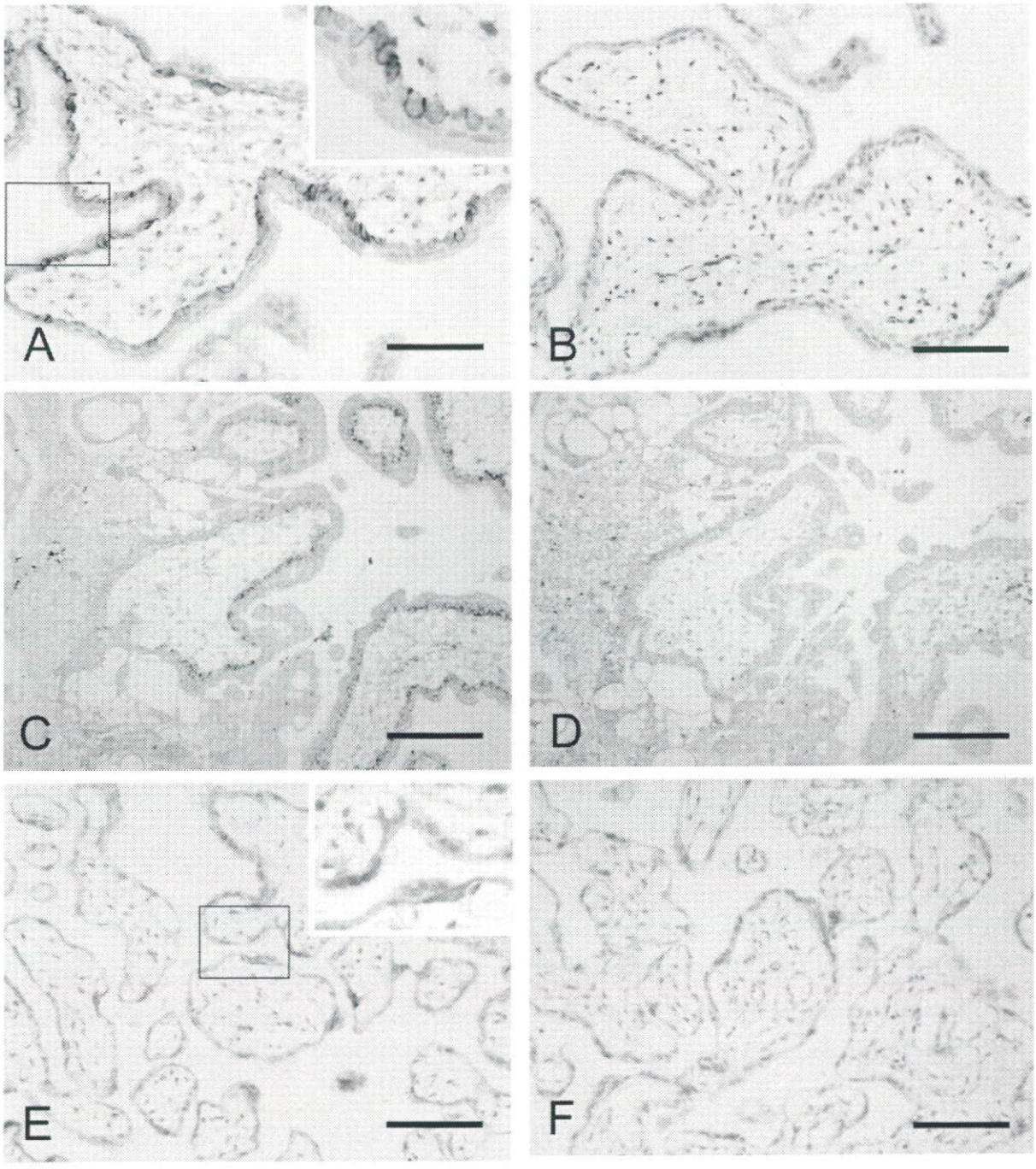

Archives of Biochemistry and Biophysics 479 (2008) 1–14

Contents lists available at ScienceDirect

Archives of Biochemistry and Biophysics

journal homepage: www.elsevier.com/locate/yabbi

LDL protein nitration: Implication for LDL protein unfolding

Ryan T. Hamilton [a], Liana Asatryan [a], Jon T. Nilsen [a], Jose M. Isas [c], Timothy K. Gallaher [a], Tatsuya Sawamura [d], Tzung K. Hsiai [b,*]

[a] Department of Pharmacology and Pharmaceutical Sciences, School of Pharmacy, University of Southern California, Los Angeles, CA 90089, USA
[b] Department of Biomedical Engineering and Division of Cardiovascular Medicine, Viterbi School of Engineering, University of Southern California, Los Angeles, CA 90089, USA
[c] Department of Biochemistry and Molecular Biology, Keck School of Medicine, University of Southern California, Los Angeles, CA 90089, USA
[d] Department of Pharmaceutical Sciences and Division of Cell Biology, Department of Bioscience, National Cardiovascular Center Research Institute, Osaka University, Japan

ARTICLE INFO

Article history:
Received 12 December 2007
and in revised form 12 July 2008
Available online 7 August 2008

Keywords:
LDL
Nitration
Oxidation
Endothelial cells

ABSTRACT

Oxidatively- or enzymatically-modified low-density lipoprotein (LDL) is intimately involved in the initiation and progression of atherosclerosis. The *in vivo* modified LDL is electro-negative (LDL^-) and consists of peroxidized lipid and unfolded apoB-100 protein. This study was aimed at establishing specific protein modifications and conformational changes in LDL^- assessed by liquid chromatography/tandem mass spectrometry (LC/MS/MS) and circular dichroism analyses, respectively. The functional significance of these chemical modifications and structural changes were validated with binding and uptake experiments to- and by bovine aortic endothelial cells (BAEC).

The plasma LDL^- fraction showed increased nitrotyrosine and lipid peroxide content as well as a greater cysteine oxidation as compared with native- and total-LDL. LC/MS/MS analyses of LDL^- revealed specific modifications in the apoB-100 moiety, largely involving nitration of tyrosines in the α-helical structures and β_2 sheet as well as cysteine oxidation to cysteic acid in β_1 sheet. Circular dichroism analyses showed that the α-helical content of LDL^- was substantially lower (~25%) than that of native LDL (~90%); conversely, LDL^- showed greater content of β-sheet and random coil structure, in agreement with unfolding of the protein. These results were mimicked by treatment of LDL subfractions with peroxynitrite ($ONOO^-$) or SIN-1: similar amino acid modifications as well as conformational changes (loss of α-helical structure and gain in β-sheet structure) were observed. Both LDL^- and $ONOO^-$-treated LDL showed a statistically significant increase in binding and uptake to- and by BAEC compared to native LDL. We further found that most binding and uptake in control-LDL was through LDL-R with minimal oxLDL-R-dependent uptake. $ONOO^-$-treated LDL was significantly bound and endocytosed by LOX-1, CD36, and SR-A with minimal contribution from LDL-R.

It is suggested that lipid peroxidation and protein nitration may account for the mechanisms leading to apoB-100 protein unfolding and consequential increase in modified LDL binding and uptake to and by endothelial cells that is dependent on oxLDL scavenger receptors.

Low density lipoprotein (LDL)[1] particles transport cholesterol, cholesterol esters, lipids, phospholipids, and are involved in the maintenance of membrane fluidity [1]. The LDL particle is comprised of lipid core and an apolipoprotein B-100 (apoB-100) moiety. The latter assumes a pentapartite structure with alternating α-helices and β-pleated sheets (α_1–β_1–α_2–β_2–α_3) [2]. α_1 anchors the protein to the lipid core; α_2 and α_3 expand and contract across the phospholipid belt of the LDL particle to stabilize electrostatic interactions, thus maintaining LDL protein structural integrity. β-sheets are structurally rigid and engaged in electrostatic interactions with the phospholipids [2].

It is widely recognized that oxidative and/or enzyme-mediated modifications of LDL are required for the particle to acquire the inflammatory properties inherent in the initiation and progression of atherosclerosis [3,4]. This notion is strengthened by the observation that post-translational modifications of apo-B100 are elevated in atherosclerotic lesions [5]. Oxidation of LDL can be carried out by transition metals, hemoglobin, myeloperoxidase, cerruloplasmin, and reactive oxygen species generated by vascular endothelium [6–8]. The oxidative modifications render the LDL particle electronegatively charged (LDL^-) as compared to native LDL (nLDL) [3,9,10]. Also, LDL^- (*in vivo* oxidatively-modified LDL) contains elevated level of lipid peroxides and aldehydes that are implicated in

* Corresponding author. Fax: +1 323 821 3897.
E-mail address: hsiai@usc.edu (T.K. Hsiai).

[1] *Abbreviations used:* LDL, low-density lipoprotein; nLDL, native LDL; tLDL, total LDL; LDL^-, negatively-charged LDL, oxidatively-modified LDL; CD, circular dichroism; SIN-1, 3-morpholino-sydnonimine; DiI, 3,3,3′,3′-tetramethylindocarbocyanine perchlorate; BAEC, bovine aortic endothelial cells; Apolipoprotein B-100, ApoB-100; LC/EIS/MS, liquid chromatography electron ion spray mass spectrometry.

0003-9861/$ - see front matter © 2008 Elsevier Inc. All rights reserved.
doi:10.1016/j.abb.2008.07.026

protein unfolding [11]. Reactive nitrogen species, especially peroxynitrite ($ONOO^-$), generated by the vascular endothelium, nitrate apo-B-100 in LDL particles [10,12–15]. Enzyme-mediated modifications of LDL—accomplished through the action of ubiquitous hydrolytic enzymes—confer atherogenic properties to the lipoprotein particles [4,16]: *s*-phospholipase A_2 [3] and its free fatty acid product [17], cholesteryl esterases [4], plasmin [18], and matrix metalloproteinase -2 and -9 [18].

This oxidative- and/or enzymatically-modified LDL possesses inflammatory properties: it activates cytokines [19] and monocyte adhesion molecules [20]. The LDL particle is internalized by cells via the ubiquitously expressed LDL receptor (LDL-R). Rather than binding to the LDL-R commonly present in cells, protein unfolding in modified LDL promotes binding to the scavenger receptors (LDL-SR) in vascular endothelial cells [21] and to CD36 in macrophages [11,22]. $ONOO^-$-modified LDL is recognized by macrophages, thus gaining further relevance in endothelial dysfunction and initiation of atherosclerosis [15,23,24]. Further, endothelial cells are involved in the initiation of atherosclerosis by the binding of modified LDL and/or apoptotic cells and inducing macrophage/monocyte chemoattractant proteins as well as inducing inflammation [25].

In this study, we assessed specific protein modifications and conformational changes of *in vivo* oxidatively-modified LDL (LDL^-) and $ONOO^-$-treated LDL by liquid chromatography/tandem mass spectrometry (LC/MS/MS) analyses and circular dichroism (CD) spectra. The significance of $ONOO^-$-driven modifications is underscored by the implication of both NADPH oxidase (a source of $O_2{}^{\cdot-}$) [10,26,27] and eNOS (a source of $^{\cdot}NO$) [28] activities in vascular endothelial dysfunction and by the fast reaction of $O_2{}^{\cdot-}$ and $^{\cdot}NO$ to yield $ONOO^-$.

Materials and methods

Chemicals

$ONOO^-$ and monoclonal nitrotyrosine antibody were purchased from Upstate Cell Signaling Solutions (UCSS, Lake Placid, NY). Bovine serum albumin, 3-morpholino-sydnonimine (SIN-1), biotin, and 3′-tetramethylindocarbocyanine perchlorate (DiI) were purchased from Sigma (St. Louis, MO). Bovine aortic endothelial cells were purchased from Cell Applications, Inc. (San Diego, CA). Lectin, like oxidized LDL receptor, was a gift from Dr. Tatsuya Sawamura (Osaka University, Japan). CD36 receptor blocking antibody, SR-A receptor blocking antibody, and LDL-R antibody were obtained from Beckman Coultier (Fullerton, California), Serotec (Raleigh, North Carolina), and Calbiochem (San Diego, California), respectively.

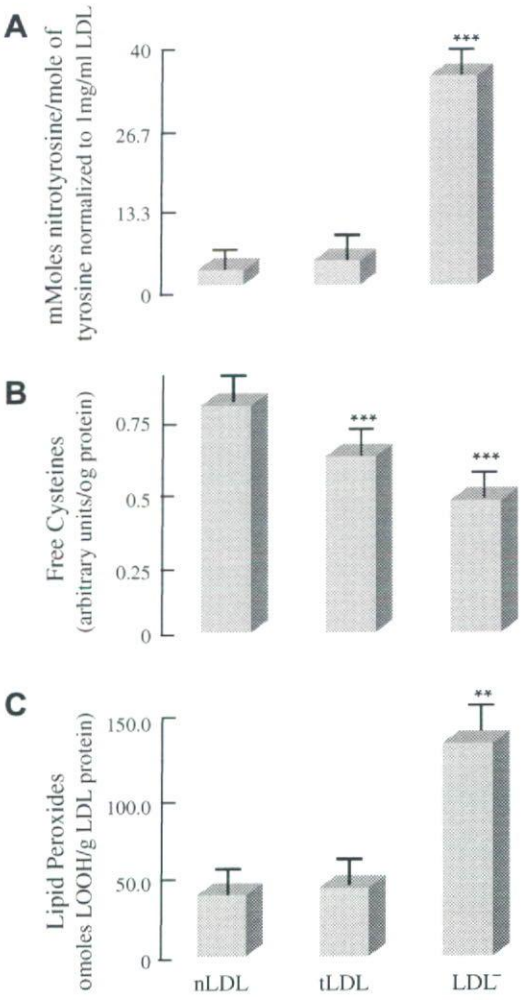

Fig. 1. Chemical modifications of *in vivo* LDL subfractions. LDL sub-fractions were isolated by anion exchange chromatography as described in Materials and methods and analyzed for (A) nitrotyrosine content, (B) free cysteine content (biotin labeling), and labeling, and (C) lipid peroxide content. ($n = 3$, $^*P < 0.05$, $^{**}P < 0.01$, $^{***}P < 0.001$).

Table 1
LC/MS/MS analyses of LDL^- Apo-B100 protein modifications

Secondary structure	Peptide	Modified AA	Sequence	MSc	Charge	XC	Δcn	Modification	% modified
α_1	276–287	NO_2-Tyr^{276}	y[a]gmvaqvtqtlk	51	2	2.8	0.4	nitrotyrosine	100 ± 0
α_1	580–589	NO_2-Trp^{583}	lVQilpw[a]eqneqv	30	2	3.0	0.2	nitrotryptophan	49.8 ± 0.6
α1	580–589	HO-Trp^{583}	lVQilpw[a]eqneqv	38	2	3.8	0.3	hydroxytryptophan	32.6 ± 1.9
α_1	655–669	NO_2-Tyr^{666}	iegnlifdpnny[a]lpk	46	2	3.3	0.4	nitrotyrosine	18.3 ± 0.7
α_1	718–732	NO_2-Tyr^{720}	aly[a]wavngqvpdgvsk	49	2	2.4	0.1	nitrotyrosine	29.9 ± 0.07
β_1	1101–115	SO_3H-Cys^{1112}	itevalmghlsc[a]dtk	84	2	4.9	0.5	cysteic acid	100 ± 0
α_2	2523–2534	NO_2-Tyr^{2524}	my[a]qmdiqqelqr	36	2	3.0	0.3	nitrotyrosine	87.1 ± 0.2
β_2	3137–3148	NO_2-Tyr^{3139}	lpy[a]tiitpplk	30	2	1.9	0.5	nitrotyrosine	60.2 ± 0.2
β_2	3292–3311	NO_2-Tyr^{3295}	vpsy[a]tlilpslelpvlhvpr	70	2	5.6	0.5	nitrotyrosine	80.4 ± 0.2
β_2	3481–3497	NO_2-Tyr^{3489}	lslesltsy[a]fsiesstk	62	2	4.7	0.7	nitrotyrosine	27.1 ± 1.1
β_2	3953–3973	HO-Phe^{3965}	dfsaeyeedgkf[a]eglqewegk	59	2	2.5	0.5	HO-phenylalanine	92.6 ± 0.9
α_3	4133–4145	NO_2-Tyr^{4141}	aasgttgty[a]qewk	46	2	2.7	0.1	nitrotyrosine	81.8 ± 0.1
			Quantification of NO_2-Y mmol NO_2-Y/(mol Y) LDL^- = 34.8 ± 1.0 tLDL = 2.0 ± 0.2 nLDL = 0.3 ± 0.1						

[a] Full annotated MS spectra are represented in the order presented in this table in Figs. 1–12 of the Supplemental section.

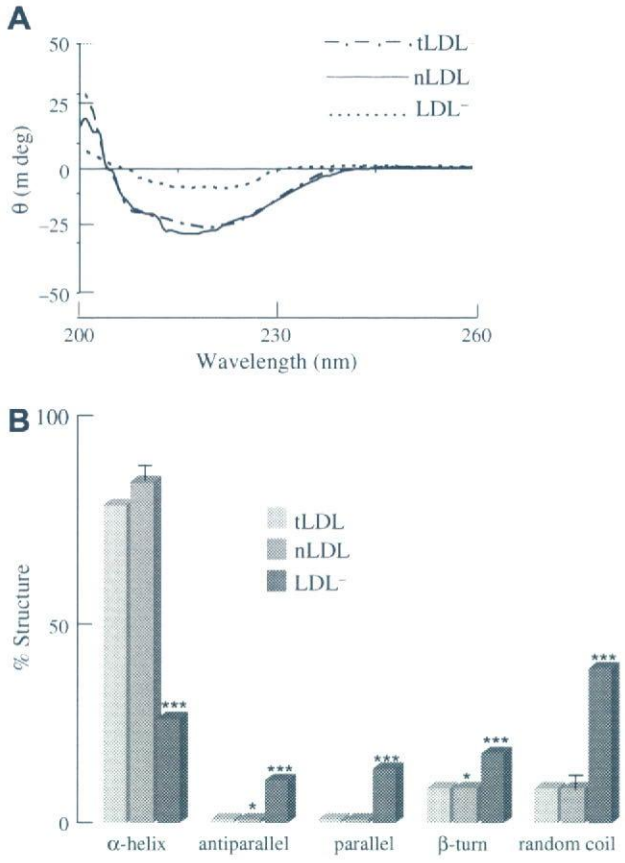

Fig. 2. Circular dichroism spectral analyses of *in vivo* LDL sub-fractions. (A) Circular dichroism spectra for different LDL sub-fractions were performed as described in Materials and methods. (B) Secondary structures of LDL sub-fractions; data were obtained from spectra in (A), which were deconvoluted for apoB-100 secondary structure. ($n = 3$, $^{*}P < 0.05$, $^{**}P < 0.01$, $^{***}P < 0.001$).

Isolation of in vivo LDL and modification of LDL and isolation of LDL⁻

Low density lipoprotein (LDL) was isolated from human plasma (USC blood bank) by density gradient ultra centrifugation and pooled from multiple expired plasma LDL donors as obtained from the USC blood bank (L-80 XP centrifuge, SW-41 rotor, Fullerton CA) [29]. LDL ($\delta = 1.019 - 1.063$) was then collected and washed with phosphate-buffered saline (PBS) several times using a Millipore (Bedford, MA) centrifugal filtering device with a 30 kDa cut-off. Anion exchange liquid chromatography using a stepwise sodium chloride gradient to isolate nLDL, LDL^{-}, and LDL^{2-} to analyze the percentage of LDL^{-}. HPLC was performed to analyze the percentage of LDL^{-}. Concentrated LDL (at 200 μg/ml) was then incubated with different concentrations of either $ONOO^{-}$ or SIN-1 for 30 min at 37 °C. Sin-1 was used as a donor of ·NO and $O_2^{\cdot -}$ to form $ONOO^{-}$ and to corroborate findings of $ONOO^{-}$-treated LDL [30]. The concentration of $ONOO^{-}$ stock was measured prior to the individual experiments using UV absorption spectra ($\lambda_{302nm} = 1.67\ mM^{-1}\ cm^{-1}$) according to the manufacturer's specification (Upstate, Lake Placid, NY).

Analysis of LDL modifications

Oxidation: LDL post-translational modifications were assessed in *in vivo* LDL subfractions (LDL) and *in vitro* $ONOO^{-}$/SIN1-treated LDL. Protein oxidation was determined by a decrease in biotin labeling to the oxidized cysteine residues. Biotin labeling was performed by incubating biotin with LDL for 1 h at 37 °C to label free unmodified cysteine residues. *Nitrotyrosine:* Two micrograms of $ONOO^{-}$-treated LDL and 10 μg of *in vivo* LDL subfractions were spotted on Millipore PVDF membranes. Two micrograms BSA nitrated with 1 mM $ONOO^{-}$ was used as a positive control. Dithionite was used to reduce nitro groups in the positive control in order to show that the binding was specific. *Dot blot analyse:* Dot blots were performed at a 1:3000 dilution in TBS-Tween for primary nitrotyrosine antibody and 1:10000 dilution for anti-mouse secondary antibody. Similar procedures were performed for 4 μg of biotin-labeled LDL with a monoclonal anti-biotin antibody (dilution at 1:10,000) and a secondary antibody (dilution at 1:10,000), (Sigma, St. Louis, MO). Dot Blots were analyzed using an ECL chemiluminescence kit (Pierce, Rockford, IL), and densitometry was performed using an NIH Scion Image Software (Scion Corp., Frederick, MD) and a product of the density and area determined. The product was also normalized to protein used for both nitrotyrosine and cysteine oxidation analysis. Total nitrotyrosine was quantified by LC/EIS/MS for $ONOO^{-}$-treated LDL samples. Western blot densities for $ONOO^{-}$-treated LDL were plotted against the quantified content of nitrotyrosine in the samples and this standard curve was used to determine the quantity of nitrotyrosine in both the *in vivo* LDL sub-fractions as well as the SIN-1 treated LDL by extrapolation of the curve. Comparison of nitrotyrosine quantities in the $ONOO^{-}$-treated LDL were comparable to the findings by Leeuwenburgh et al. after normalization to a 1 mg/ml solution [5].

Lipid peroxide measurements

Lipid peroxidation and cholesterol hydroperoxides was measured by the leucomethylene blue assay with *tert*-butyl-hydroperoxide as a standard. LMB cocktail consisted of a 0.05 M pH 5 potassium phosphate buffer with 1.4 g of Triton-X-100 and 5 mg of hemoglobin to 100 ml total volume. Five micrograms of LMB was diluted in 8 ml of dimethylformamide and 0.8 ml of LMB dimethylformamide cocktail was added to 10 ml of potassium phosphate buffer. Fifty micrograms of LDL were incubated with 150 μl of LMB cocktail for 1 h to a final volume of 200 μl in 96 well plates. Total tryptophan in apoB-100 was relatively small and any tryptophan hydroperoxides should only be minor contaminants The colorimetric assay was measured at 650 nm after 1 h incubation at room temperature with a leucomethylene blue cocktail mixture [3]. Molar concentrations of lipid peroxides were determined from a standard curve and total yield of LOOH determined as a ratio of μmol LOOH/g of LDL protein.

Analysis of specific sites of LDL protein nitration

LDL^{-} and nLDL were isolated from *in vivo* LDL by HPLC using a stepwise NaCl gradient as previously described [29]. For 100 μM $ONOO^{-}$-treated LDL, tLDL was analyzed for oxidative modifications. Liquid chromatography tandem mass spectrometry (LC-MS/MS) was performed using a ThermoFinnigan Surveyor MS-Pump with a BioBasic-18 100 × 0.18 mm reverse phase capillary column. The column was equilibrated for 5 min at 1.5 μl/min with 95% solution A and 95% solution B (A, 0.1% formic acid in water; B, 0.1% formic acid in acetonitrile) and linear gradient was initiated 5 min after sample injection with a ramp to from 95% A to 35% A and 65% B after 50 min and 20% A and 80% B after 60 min. Analysis was obtained by the ThermoFinnigan LCQ Deca XP Plus ion trap mass spectrometer, equipped with a nanospray ion source (ThermoFinnigan) that employed a 4.5 cm metal needle (Hamilton, 950-00954), in a data-dependent acquisition mode. Electrical contact and voltage application to the probe tip were established via the nanoprobe assembly. Spray voltage was set at 2.9 kV and heated capillary temperature at 190 °C. Mass spectra were ac-

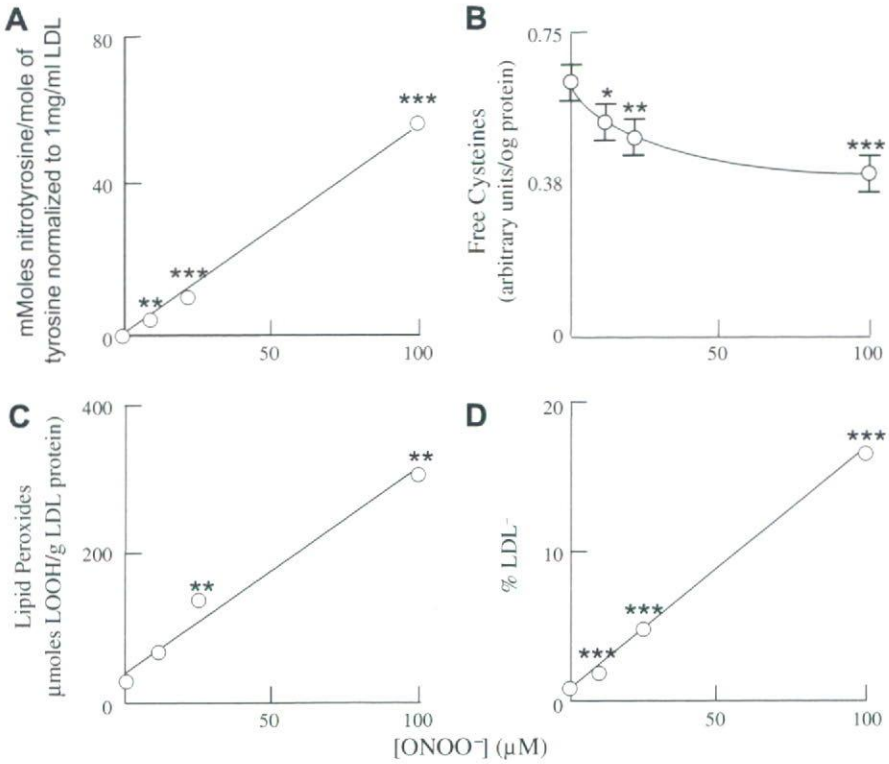

Fig. 3. $ONOO^-$-modified LDL. LDL samples were supplemented with different amounts of $ONOO^-$ and analyzed for (A) nitrotyrosine, (B) free cysteine (after biotin labeling), (C), lipid peroxides, and LDL^- content (percentage). ($n = 3$, $^*P < 0.05$, $^{**}P < 0.01$, $^{***}P < 0.001$).

Table 2
LC/MS/MS analyses of $ONOO^-$-modified LDL Apo-B100

Secondary structure	Peptide	Modified AA	Sequence	MSc	charge	XC	Δcn	Modification	% modified
α_1	101–110	NO_2-Tyr^{103}	EVY[a]GFNPEGK	29	1	1.7	0.4	Nitrotyrosine	49.9 ± 1.7
α_1	401–427	NO_2-Tyr^{413}	VHANPLLIDWTY[a]LVALIPEPSAQQLR	33	2	2.6	0.3	Nitrotyrosine	53.7 ± 1.4
α_1	655–669	NO_2-Tyr^{666}	IEGNLIFDPNNY[a]LPK	28	2	2.8	0.4	Nitrotyrosine	81.5 ± 3.3
α_2	2523–2534	NO_2-Tyr^{2524}	MY[a]QMDIQQELQR	65	2	3.7	0.4	Nitrotyrosine	66.6 ± 5.9
β_2	3481–3497	NO_2-Tyr^{3489}	LSLESLTSY[a]FSIESSTK	20	2	0.2	2.0	Nitrotyrosine	41.3 ± 0.6
β_2	3767–3772	NO_2-Tyr^{3771}	EIQIY[a]K	25	1	0.1	1.3	Nitrotyrosine	29.1 ± 0.7
β_2	3953–3973	HO-Phe^{3965}	DFSAEYEEDGKFEGLQEWEGK	30	2	3.7	0.4	HO-phenylalanine	86.3 ± 0.2
α_3	4088–4098	NO_2-Tyr^{4088}	Y[a]HWEHTGLTLR	28	2	2.1	0.3	Nitrotyrosine	95.3 ± 0.8
			Quantification of NO_2-Y mmol NO_2-Y/(mol Y) 54.2 ± 1.3						

[a] Full annotated MS spectra are represented in the order presented in this table in Figs. 13–20 of the Supplemental section.

quired at 400–2000 *m/z* using a Top five method where the five most intense ions for the full scan were subjected to collision induced dissociation, using helium (ms/ms). Peptide identification was achieved using Mascot 1.9 search software (Matrix Science) with confirmatory or complementary analyses by TurboSequest as implemented in the Bioworks Browser 3.2, build 41 (ThermoFinnigan). Spectra were searched against the NCBI human genome database, NCBI build 35. Aromatic nitration and hydroxylation as well cysteine oxidation were assessed using Mascot 1.9 (Matrix Science) for cysteic acid, nitrotyrosine and nitrotryptophan, with confirmatory or complementary analyses that employed TurboSequest as implemented in the Bioworks Browser 3.2, build 41 (ThermoFinnigan) [31,32]. In addition to cysteic acid (+48 Da), nitrotyrosine (+45 Da) and nitrotryptophan (+45 Da), Sequest was used to assess the presence of single or doubly oxidized cysteine (+16 and +32, respectively) as well as tryptophan with both a nitration and oxidation (+61). Quantification of nitrated peptides was carried out by analysis of peak nitration to peak unmodified plus peak modified peptides (NO_2-peptide/(NO_2-peptide + unmodified peptide). Further positive peptides were analyzed against their y- and b-ions to insure that peptides measured were present and not false positives. They were further analyzed against their peak height to noise ratio.

Circular dichroism spectral analysis of protein structure

Circular dichroism (CD) allows for probing the secondary structure content of proteins. The CD spectrum of modified LDL provides a means to determine the conformational changes of secondary structure in apoB-100 (α-helix, anti-parallel and parallel β-sheet, β-turn, and random coil). *In vivo* isolated LDL and 100 µM $ONOO^-$-treated LDL sub-fractions of LDL isolated from HPLC were concentrated and dialyzed to a 0.1 mg/ml solution in chloride free phosphate buffer saline for CD analysis. CD spectra were measured at least ten times to determine the protein structure. Different secondary structures are represented by the spectrum between 200 and 260 nm. Deconvolution analysis using CD spectra software (CDNN) allowed for assessment of the percent structural integrity in the LDL sub-fractions of modified LDL.

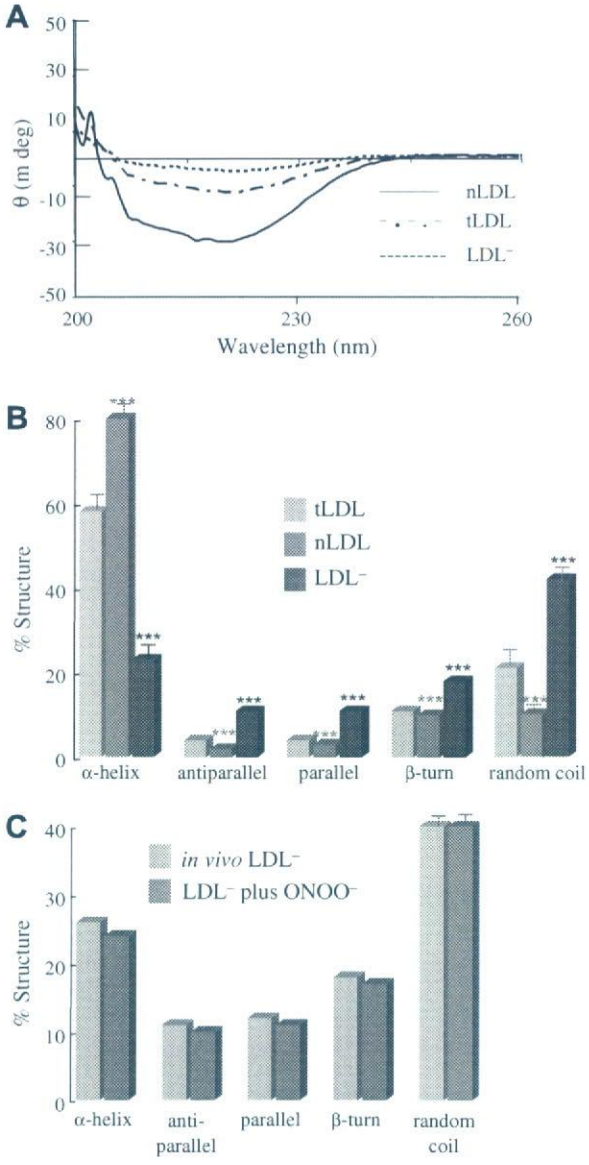

Fig. 4. Circular dichroism spectral analyses of $ONOO^-$-modified LDL. tLDL was treated with 10 μM $ONOO^-$ as described in Materials and methods); the $ONOO^-$-treated tLDL was fractionated into nLDL and LDL^- components and CD spectra were determined. (A) Circular dichroism spectra of LDL sub-fractions. (B) Secondary structure of different LDL sub-fractions. CD deconvolution software wasused to determine the changes in the structures of the LDL sub-fractions. (C) Comparison of secondary structure components in *in vivo* LDL^- and LDL^- from $ONOO^-$-treated tLDL. Data taken from Fig. 2B (for *in vivo* LDL^-) and Fig. 4B (LDL^- fraction of the $ONOO^-$-treated tLDL). ($n = 3$, $^*P < 0.05$, $^{**}P < 0.01$, $^{***}P < 0.001$).

Endothelial cell culture

Bovine aortic endothelial cells (BAEC) between passages five and nine were grown to confluent monolayers in high glucose (4.5 g/l) DMEM (Dulbecco's Modified Eagle's Medium) supplemented with 10% heat-inactivated fetal bovine serum (Gemcell, West Sacramento, CA) and 100 U/ml penicillin–streptomycin (Irvine Scientific, Santa Ana, CA), for 48 h in 5% CO_2 at 37 °C.

Binding and uptake of LDL particles

Control and 100 μM $ONOO^-$-supplemented LDL particles were treated with 75 mg/ml DiI overnight. DiI-labeled LDL particles were ultracentrifuged, collected, dialyzed, and sterilized to remove the DiI particulate [33]. BAEC were treated with 10 μg/ml DiI-labeled LDL at 0 °C for 90 min or at 37 °C for 4 h for LDL binding or uptake experiments, respectively [33]. Cells were also treated with10 μg/ml DiI-labeled LDL with 200 μg/ml of excess unlabeled LDL as a control to exclude DiI labeling of cell membranes and for LDL binding and uptake specificity [33]. Cells were washed thoroughly with DMEM three times after treatment, washed in PBS three times, fixed in paraformaldehyde for 10 min at room temperature, and washed six more times with PBS. Cells were mounted in DAPI-containing mounting medium and visualized using an Axiom 200 M Zeiss Fluorescent Microscope (Zeiss, Thornwood, NY) was performed using a DAPI filter for the nucleus and CY3 filter for the DiI-labeled LDL. Quantification of mean intensity and image analysis were assessed by slidebook software (Santa Monica, CA).

Receptor blocking

BAEC were pre-treated for 1 h with a 1:250 dilution of receptor blocking antibodies to LOX-1, CD36, SR-A, and LDL-R to determine receptor involvement in control- and $ONOO^-$-LDL binding and uptake. BAEC were pre-treated with receptor blocking antibodies as follows: (1) no receptor blocking (all active), (2) All receptors blocked (all four inactive), (3) all receptor blocking except LOX-1 (LOX-1 active), (4) all receptor blocking except CD36 (active CD36), (5) all receptor blocking except SR-A (Active SR-A), and (6) all receptor blocking except LDL-R (active LDL-R). Uptake and binding of DiI-labeled control- and $ONOO^-$-LDL were performed by the methods described above.

Statistical analysis

Data were expressed as mean ± SD and compared among separate experiments ($n = 3$). For comparisons between two groups, two-sample independent-group *t*-tests were used (one tail and type three *t*-test analysis). Comparisons of multiple values were made by one-way analysis of variance (ANOVA), and statistical significance among multiple groups determined by the Tukey test (for pair-wise comparisons of means between control and treatments). *P*-values of <0.05 are considered statistically significant.

Results

Post-translational modifications of in vivo LDL^-

In vivo native LDL (nLDL) and LDL^- were isolated from total-LDL (tLDL) using anion exchange chromatography as described in Materials and methods. The average of LDL^- isolated from tLDL *in vivo* was 1.05 ± 0.05% of the total-LDL protein for the purposes of these experiments. LDL nitration was assessed by immunoreactivity to nitrotyrosine antibody (Fig. 1A). While nitrotyrosine was not detectable in either nLDL or tLDL, it was prominent in the LDL^- fraction ($n = 3$; $P < 0.001$; Fig. 1A). Oxidation of the nine free cysteine residues in the *in vivo* LDL sub-fractions was assessed by biotin labeling of free cysteine (Fig. 1B). LDL^- harbored a significantly lower level of free cysteine in comparison with nLDL and tLDL: nLDL < tLDL < LDL^-) ($n = 3$, $P < 0.001$), thus suggesting an elevated amount of cysteine oxidation in LDL^- (Fig. 1B). Also worth noting was a threefold increase in lipid peroxides in LDL^- in comparison with nLDL and tLDL ($n = 3$, $P < 0.001$) (Fig. 1C).

LC/MS/MS analyses of *in vivo* LDL-revealed specific modifications in the apoB-100 moiety (Table 1): tyrosine (Tyr), tryptophan (Trp), cysteine (Cys), and phenylalanine (Phe) underwent nitration/oxidation in both α helices and β-sheets; namely, α_1 ($Tyr^{276,666,720}$, Trp^{583}), α_2 (Tyr^{2523}), β_2/α_3(Phe^{3969}), β_1 (Cys^{1112}), α_3 (Tyr^{4141}), and β_2 ($Tyr^{3139,3295,3489}$) (Table 1) as corroborated by the Mascot and

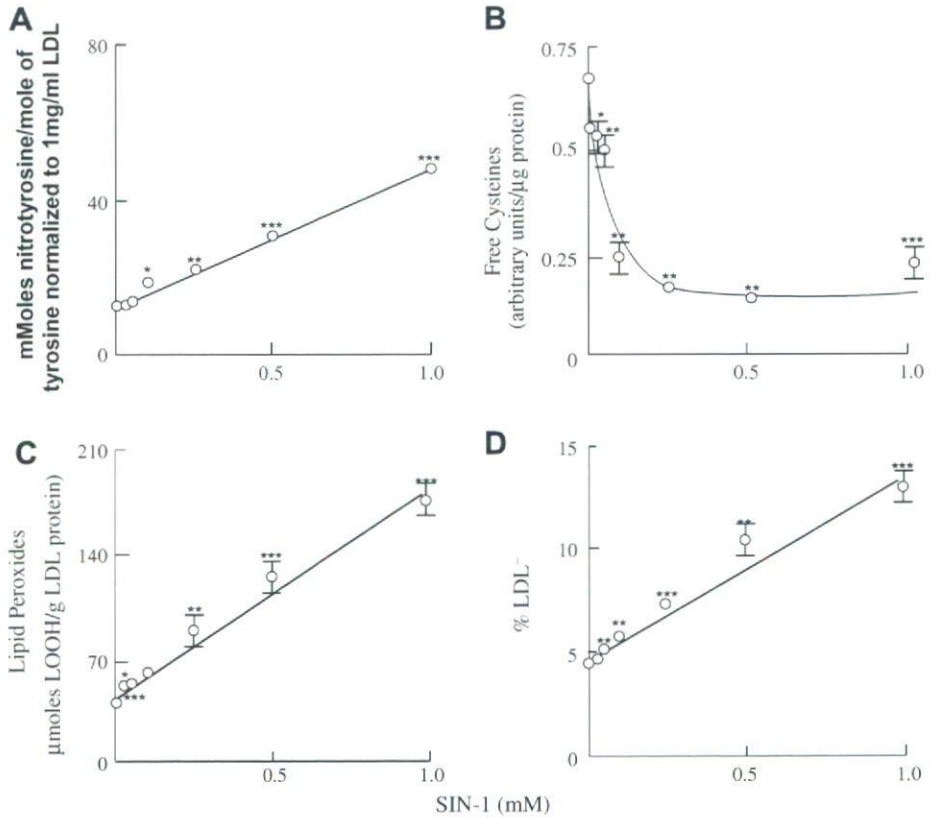

Fig. 5. SIN-1-modified LDL. LDL particles were incubated with different amounts of SIN-1 and analyzed for (A) nitrotyrosine, (B) free cysteine, (C) lipid peroxides, and (D) percentage of LDL⁻ as described in Materials and methods section. ($n = 3$, $^{*}P < 0.05$, $^{**}P < 0.01$, $^{***}P < 0.001$).

Sequest scores as well as analysis of peptide and peptide ions masses. These data suggested a large extent of protein modification in the electronegative subfraction or modified LDL subfraction *in vivo* which are consistent with a purification of the *in vivo* oxLDL (LDL⁻). It was further noted that the nitration levels were similar in content to that of 100 μM $ONOO^-$-treated LDL. Cys^{1112} in β_1 sheet was oxidized to cysteic acid. Modifications of these peptides are shown in the supplemental (Supplemental Figs. 1–12) and indicate that spectra are accurate.

Circular dichroism and protein post-translational modifications

Previous studies have suggested that LDL⁻ had significantly unfolded α-helical structure [11,34]. Circular dichroism analysis was used in order to establish an association between specific LDL protein modifications and protein structure [3,11,34]. *In vivo* LDL subfractions (Fig. 2A, B) displayed a decrease in optical rotativity at 200–260 nm from LDL⁻ to tLDL to nLDL (Fig. 2A). Increasing optical rotativity at the 220 nm valley reflects a loss in α-helical character and an increase in β-structural components as determined by deconvolution (Fig. 2B). Deconvolution analysis using CD spectra software (CDNN) determined the percent structural integrity of the aforementioned components in LDL sub-fractions of *in vivo* modified LDL. The α-helical content in nLDL (~90%) was largely higher than that in LDL⁻ (~25%), thus suggesting substantial protein unfolding in the latter. These data suggest an association between α-helical nitration (Table 1), lipid peroxidation (Fig. 1C), and protein unfolding (Fig. 2) in LDL⁻.

Characteristics of $ONOO^-$-modified LDL

Treatment of LDL with $ONOO^-$ induced tyrosine nitration in apoB-100 protein in a dose-dependent manner (Fig. 3A; $n = 3$; $P < 0.01$). Upon analysis of total mmol of nitrotyrosine to tyrosine precursor, these data for $ONOO^-$-treated LDL were similar to the work by Leeuwenburgh et al. [5]. Densitometry analysis of biotin labeling of free cysteine showed an exponential decrease in the level of free cysteine, thus suggesting increased cysteine oxidation in response to $ONOO^-$ treatment ($n = 3$, $P < 0.001$) (Fig. 3B). Treatment of LDL with $ONOO^-$ induced a dose-dependent accumulation of lipid peroxides in LDL (Fig. 3C). HPLC analysis revealed a dose-dependent linear increase in the percentage of LDL⁻ in response to $ONOO^-$ treatment (Fig. 3D); this increase was paralleled by an increase in nitrotyrosine- (Fig. 3A) and lipid peroxide (Fig. 3C) content. Oxidized lipid-derived aldehydes were also significantly elevated in response to $ONOO^-$ treatment (data not shown). It may be surmised that both lipid peroxides and nitrotyrosine formation are involved in $ONOO^-$-induced modification of LDL to an atherogenic form (LDL⁻).

Table 2 lists the nitration and oxidation sites in the apoB-100 protein upon treatment with 100 μM $ONOO^-$: $\alpha_1(Tyr^{103,413,666})$, α_2 (Tyr^{2524}), β_2 ($Tyr^{3490,3791}$), β_2/α_3 (Phe^{3965}), and α_3 (Tyr^{4088}). Neither *in vivo* LDL⁻ (Table 1) nor $ONOO^-$-treated LDL (Table 2) showed nitration of β_1. Similarly to *in vivo* LDL⁻, $ONOO^-$ treatment elicited β_2 nitration at Tyr^{3490} (in addition to Tyr^{3791}). The phenylalanine residue between β_2 and α_3 underwent hydroxylation as also observed in *in vivo* LDL⁻. These data strengthen the notion that *in vivo* LDL⁻ may originate from $ONOO^-$-driven modifications at specific sites in apoB-100 protein. Modifications of the peptides shown above are described in the supplemental (Supplemental Figs. 13–20).

Circular dichroism analysis of $ONOO^-$-treated LDL

$ONOO^-$-treated LDL (Fig. 4A) displayed a decrease in optical rotativity at 200–260 nm for LDL⁻ as compared to nLDL. There was a

distinctive difference in the CD spectra for LDL sub-fractions at 220 nm (LDL^- > tLDL > nLDL). As mentioned above, increasing optical rotativity at 220 nm reflects a loss in α-helical structure and an increase in β-sheet structure that was confirmed by CD deconvolution software (CDNN) assessing the percent structural integrity of the different LDL sub-fractions components of $ONOO^-$-modified LDL (Fig. 4B). Interestingly, the percentage of structural components in *in vivo* LDL^- and that of $ONOO^-$-treated LDL were similar (Fig. 4C).

SIN-1-modified LDL

Because atherosclerotic lesions have increased activities of iNOS/eNOS and NADPH oxidase, a flux of ·NO and $O_2^{\cdot -}$ (to yield $ONOO^-$) may be mimicked by SIN-1 and may further support findings by our laboratory showing increased nitration at bifurcations where oscillatory flow occurs and where atherosclerosis is prone to develop [15]. Nitrotyrosine- (Fig. 5A) and lipid peroxide (Fig. 5C) accumulation as well as the percentage of LDL^- formation (Fig. 5D) following incubation of LDL with SIN-1 were similar to those observed with $ONOO^-$ (Fig. 3). SIN-1 also induced an oxidation of cysteine residues (Fig. 5B) greater than that obtained with $ONOO^-$ (Fig. 3B).

Binding and uptake of $ONOO^-$-modified LDL

The biological significance of modified LDL was assessed with respect to LDL binding to- (Fig. 6) and uptake by (Fig. 7) bovine aortic vascular endothelial (BAEC) cells. Binding experiments, performed at 0 °C, are shown for DiI-labeled LDL (Fig. 6A) and DiI-

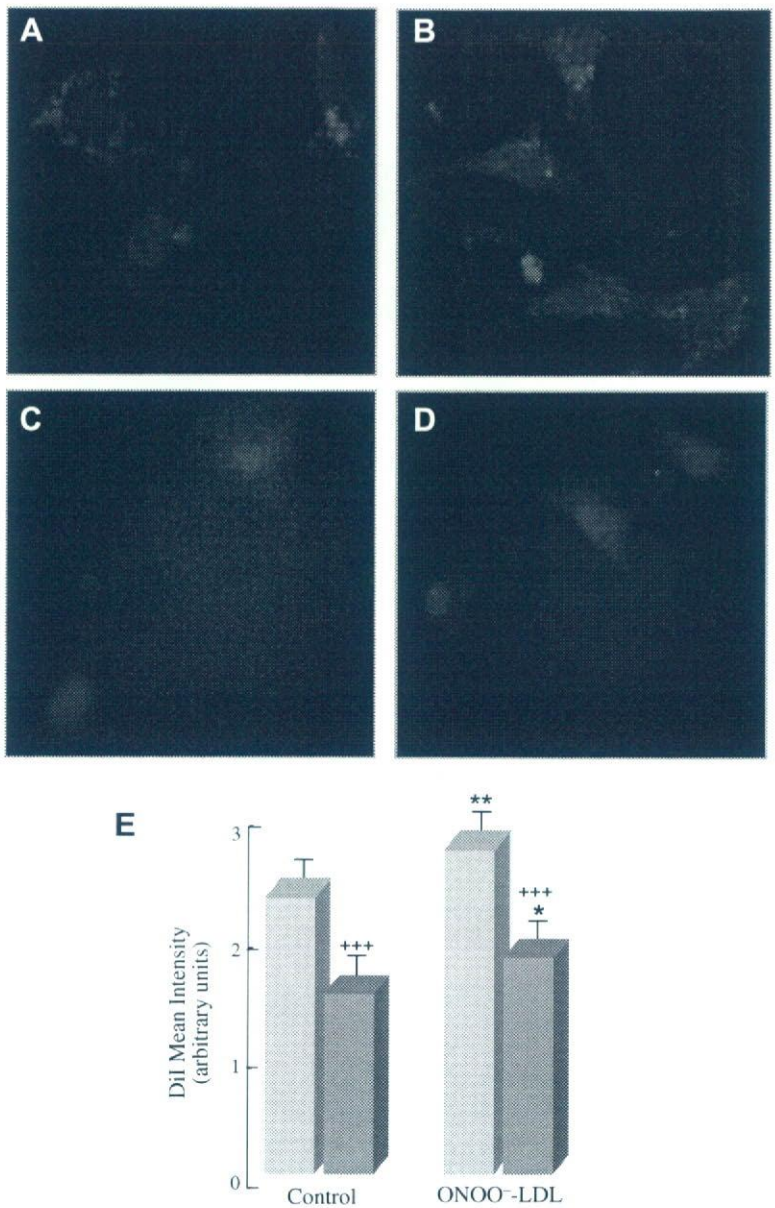

Fig. 6. Binding of $ONOO^-$-modified LDL. LDL binding experiments were performed at 0 °C for 90 min with the following conditions: (A) control-LDL 10 μg/ml DiI-LDL, (B) $ONOO^-$-treated LDL 10 μg/ml DiI-PN-LDL, (C) control-LDL 10 μg/ml DiI-LDL + 200 μg/ml unlabeled control-LDL, and (D) $ONOO^-$-treated LDL 10 μg/ml DiI-PN-LDL + excess unlabeled $ONOO^-$-treated LDL 200 μg/ml. Binding mean intensity of DiI-labeled LDL was quantified using Axiom 200 M Zeiss Fluorescent Microscope (E). Experiments were performed in triplicate and statistical significance to control-LDL and to the excess unlabeled LDL ($P < 0.01$) was determined. ($n = 3$, $^{+}P < 0.05$, $^{**,++}P < 0.01$, $^{+++,***}P < 0.001$).

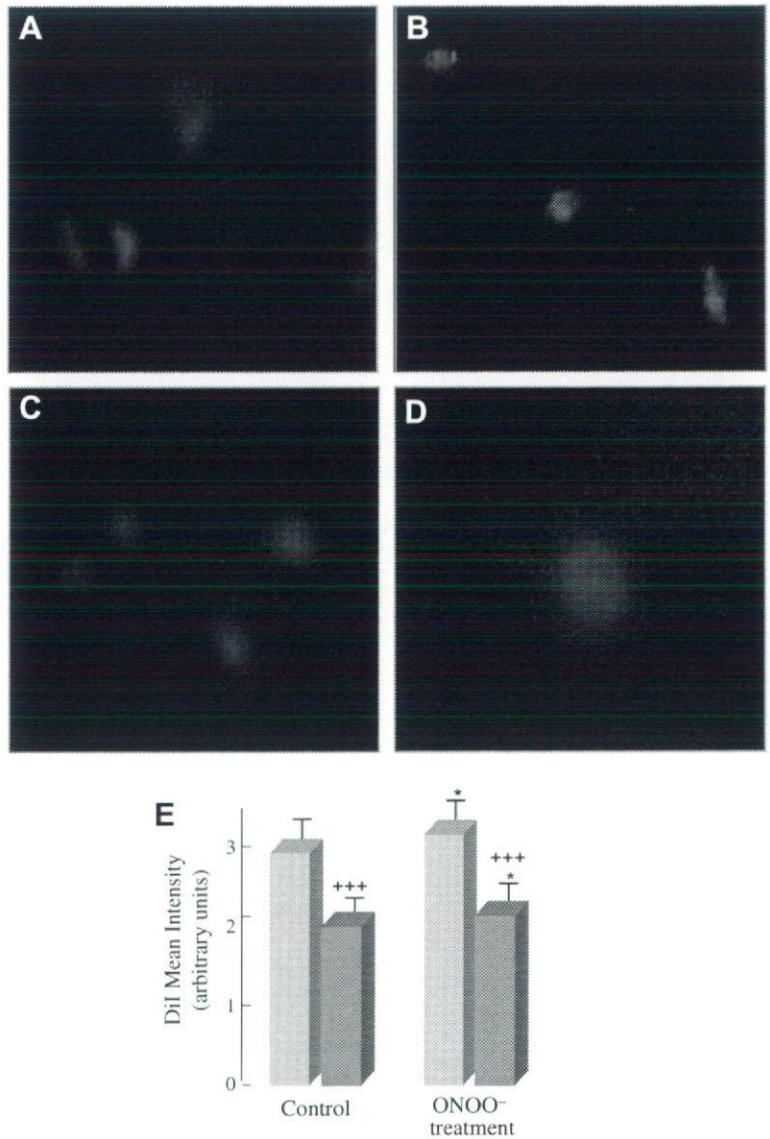

Fig. 7. Uptake of $ONOO^-$-modified LDL. LDL uptake experiments were performed at 37 °C for 4 h with the following conditions; (A) control-LDL 10 μg/ml DiI-LDL, (B) $ONOO^-$-treated LDL 10 μg/ml DiI-PN-LDL, (C) control-LDL 10 μg/ml DiI-LDL + 200 μg/ml unlabeled control-LDL, and (D) $ONOO^-$-treated LDL 10 μg/ml DiI-PN-LDL + excess unlabeled $ONOO^-$-treated LDL 200 μg/ml (D). Uptake mean intensity of DiI-labeled LDL was quantified using Axiom 200 M Zeiss Fluorescent Microscope (E). Experiments were performed in triplicate and statistical significance to control-LDL (*) and to the excess unlabeled LDL (+) was determined. ($n = 3$, $^{+,*}P < 0.05$, $^{++,**}P < 0.01$, $^{+++,***}P < 0.001$).

labeled, $ONOO^-$-treated LDL (Fig. 6B). Similar approaches with an excess of 200 μg/ml unlabeled LDL were used to rule out DiI labeling of cell membranes and ascertain LDL binding specificity (Fig. 6C, D). Analysis of the mean fluorescence intensity indicated that binding of $ONOO^-$-treated LDL was stronger than that of control LDL (Fig. 6E).

Uptake experiments, performed at 37 °C, are shown in Fig. 7 with a similar approach to that in Fig. 6: DiI-labeled LDL (Fig. 7A) and DiI-labeled, $ONOO^-$-treated LDL (Fig. 7B). As with binding experiments, uptake of $ONOO^-$-treated LDL was slightly higher than that of native LDL (Fig. 7E). The stronger binding and uptake of $ONOO^-$-treated LDL may suggest alternate uptake mechanisms as well as an increased uptake of unfolded proteins.

In the presence of a 20-fold excess of native LDL (Figs. 6C and 7C) or $ONOO^-$-treated LDL (Figs. 6D and 7D), respectively, binding and uptake were significantly inhibited (Figs. 6E and 7E), thus suggesting that LDL is binding to- and taken up by cells rather than nonspecific labeling of BAEC plasma membranes with DiI.

Receptor-dependent binding and uptake of control- and $ONOO^-$-LDL

Receptor-dependent binding (Figs. 8 and 9) and uptake (Figs. 10 and 11) of control- (Figs. 8 and 10) and $ONOO^-$-LDL (Figs. 9 and 11) was determined by receptor blocking of LOX-1, CD36, SR-A, and LDL-R with receptor blocking antibodies and by determining the amount of DiI-control-LDL and DiI-$ONOO^-$-LDL mean binding and uptake intensities. Analysis of control-LDL showed that the majority of the control lipoprotein binding was initiated by LDL-R (Fig. 8E, G, $P < 0.01$); however there were minimal binding differences between all receptors blocked in the presence of active LOX-1 (Fig. 8B, G), CD36 (Fig. 8C, G), and SR-A (Fig. 8D, G). However, LDL-R was not completely involved in

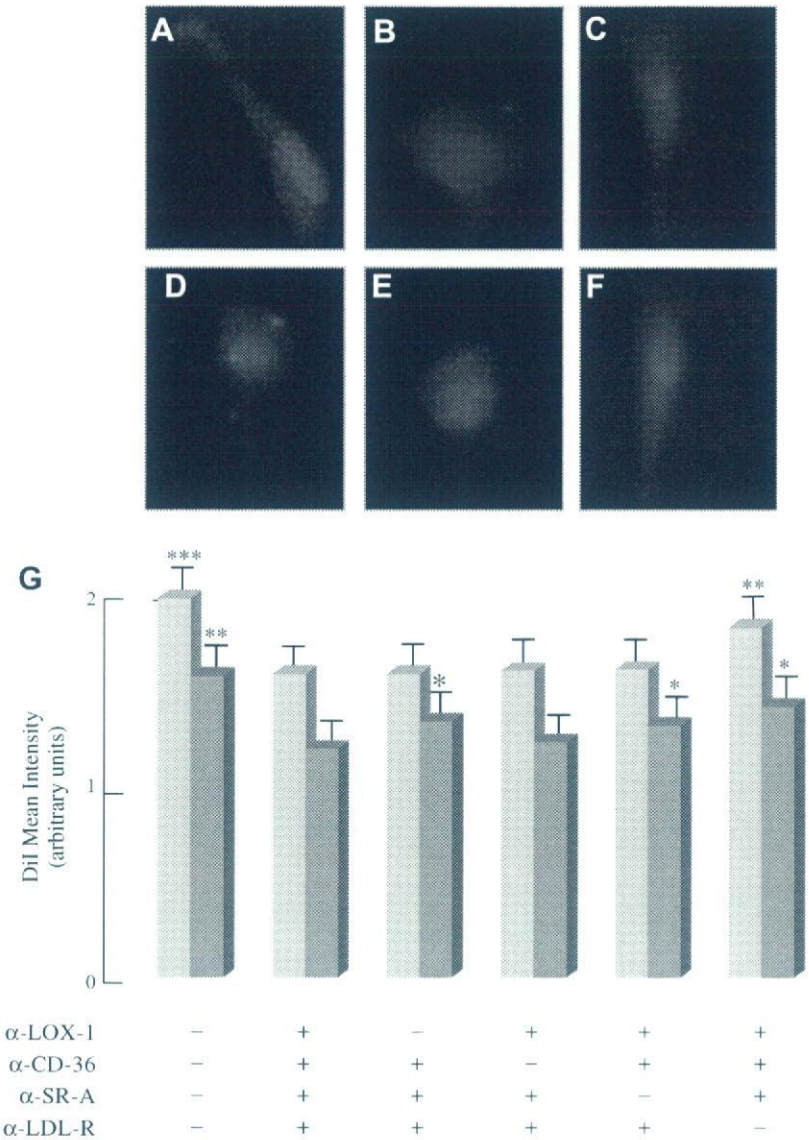

Fig. 8. Binding of control-LDL after receptor blocking. LDL receptor blocking was performed for 1 h at 37 °C and binding was determined at 0 °C with 10 μg/ml Dil-control-LDL and 10 μg/ml Dil-control-LDL with 200 μg/ml excess unlabeled LDL for 90 min by the following conditions; (A) no receptor blocking with 10 μg/ml Dil-control-LDL, (B) all four receptor's blocked with 10 μg/ml Dil-control-LDL (C) active LOX-1, (D) active CD36 with 10 μg/ml Dil-control-LDL, (E) active SR-A with 10 μg/ml Dil-control-LDL, and (F) active LDL-R with 10 μg/ml Dil-control-LDL. Binding mean intensity of Dil-control-LDL was quantified using Axiom 200 M Zeiss Fluorescent Microscope (G). Images are not shown for excess unlabeled control-LDL but intensities were quantified. Experiments were performed in triplicate and statistical significance was determined to all receptors blocked to determine receptors significantly involved in the binding of Dil-labeled control-LDL ($n = 3$, $^{*}P < 0.05$, $^{**}P < 0.01$, $^{***}P < 0.001$). ▒ – 10 mg/ml Dil-labeled control-LDL ■ – 10 mg/ml Dil-labeled control-LDL + 200 mg/ml excess unlabeled control-LDL.

the binding of control-LDL since active LDL-R was unable to completely restore binding to no receptor blocking (Fig. 8A, G). Incubating cells with excess unlabeled LDL was able to reduce the binding intensity of Dil-LDL suggesting that Dil was only minimally labeling the membranes and was not the majority of the labeling. These findings also demonstrate that control-LDL is bound to the non-atherogenic LDL-R with minimal binding from the three oxLDL-R, thus suggesting that the small amount of oxLDL *in vivo* may be binding to scavenger receptors *in vitro*.

$ONOO^-$-modified LDL was significantly bound by LOX-1 (Fig. 9C, G, $P < 0.05$), CD36 (Fig. 9D, G, $P < 0.001$) and SR-A (Fig. 9E, G, $P < 0.01$) with SR-A and CD36 having the largest impact on binding whereas active LDL-R had no impact on LDL binding (Fig. 9F, G). These findings suggest that $ONOO^-$-treated LDL is not binding through an aggregated-LDL-R-dependent mechanism but rather by each of the three scavenger receptors (LOX-1, CD36, and SR-A).

Receptor-dependent uptake of control-LDL (Fig. 10) demonstrated that the particle is taken up significantly by LDL-R (Fig. 10F, G $P < 0.001$), whereas there is minimal involvement with LOX-1 (Fig. 10C, G), CD36 (Fig. 10D, G) and SR-A (Fig. 10E, G) scavenger receptors. These findings further support the motion that control-LDL has minimal modified LDL and is minimally atherogenic as compared to $ONOO^-$-LDL.

The receptor-dependent uptake of $ONOO^-$-treated LDL was significantly elevated for LOX-1 (Fig. 11C, G, $P < 0.05$), CD36 (Fig. 11D, G, $P < 0.01$), SR-A (Fig. 11E, G, $P < 0.001$), whereas LDL-R (Fig. 11F, G) was not significantly different from all receptors blocked suggesting that $ONOO^-$-LDL is not internal-

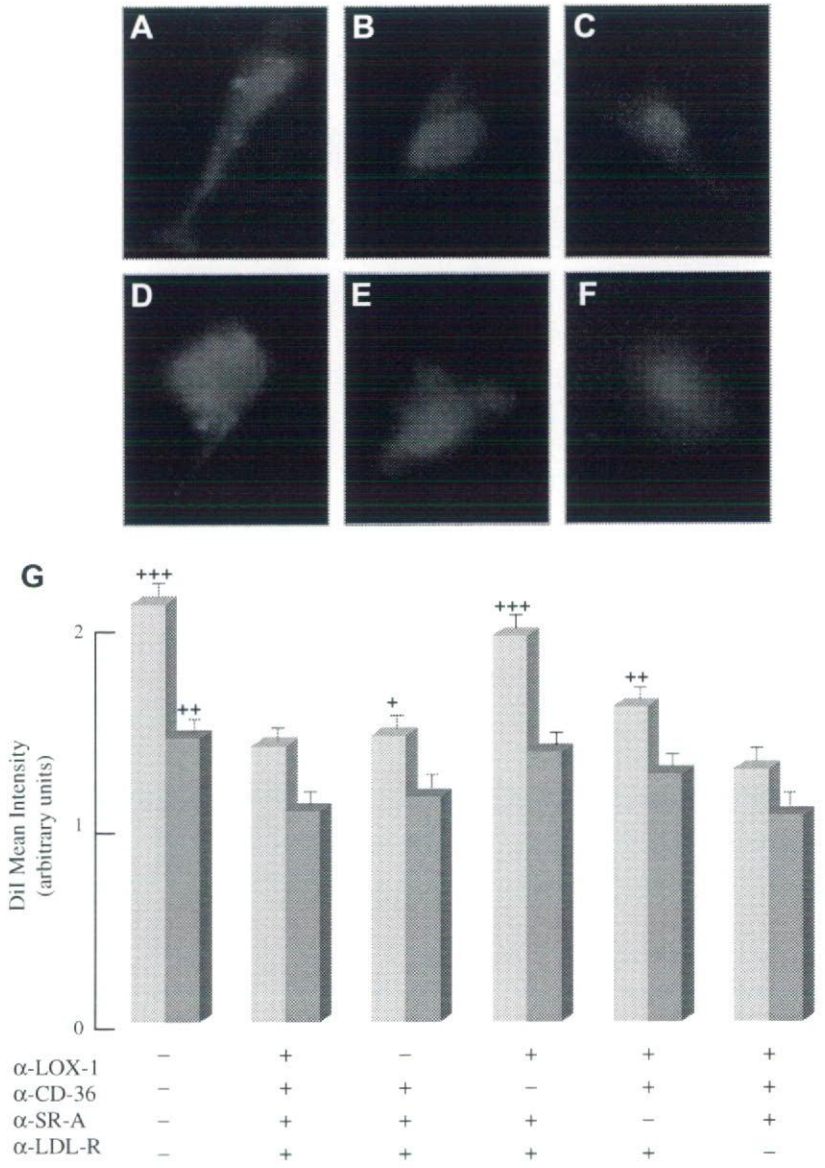

Fig. 9. Binding of ONOO⁻-LDL after receptor blocking. LDL receptor blocking was performed for 1 h at 37 °C and binding was determined at 0 °C with 10 μg/ml DiI-ONOO⁻-LDL and 10 μg/ml DiI-ONOO⁻-LDL with 200 μg/ml excess unlabeled LDL for 90 min by the following conditions; (A) no receptor blocking with 10 μg/ml DiI-ONOO⁻-treated LDL, (B) all four receptor's blocked with 10 μg/ml DiI-ONOO⁻-treated LDL (C) active LOX-1, (D) active CD36 with 10 μg/ml DiI-ONOO⁻-treated LDL, (E) active SR-A with 10 μg/ml DiI-ONOO⁻-treated LDL, and (F) active LDL-R with 10 μg/ml DiI-ONOO⁻-treated LDL. Binding mean intensity of DiI-ONOO⁻-treated LDL was quantified using Axiom 200 M Zeiss Fluorescent Microscope (G). Images are not shown for excess unlabeled ONOO⁻-treated LDL but intensities were quantified. Experiments were performed in triplicate and statistical significance was determined to all receptors blocked to determine receptors significantly involved in the binding of DiI-labeled ONOO⁻-LDL ($n = 3$, $^{*}P < 0.05$, $^{**}P < 0.01$, $^{***}P < 0.001$). ▒ – 10 mg/ml DiI-labeled ONOO⁻-treated LDL, ■ – 10 mg/ml DiI-labeled ONOO⁻-treated LDL + 200 mg/ml excess unlabeled ONOO⁻-treated LDL.

ized through an aggregated-LDL uptake mechanism. These findings further support the atherogenic character of ONOO⁻-treated LDL.

Discussion

LDL⁻ may be viewed as a circulating, atherogenic form of LDL *in vivo* and it harbors secondary structural changes in apoB-100 that encompass a significant loss of α-helical structure and increase in β-sheet structure [3]. This study addresses (a) the chemical modifications and structural changes inherent in LDL⁻ formation, (b) a functional role for ONOO⁻ in LDL⁻ formation, and (c) the occurrence of specific cellular receptors for LDL⁻.

Chemical modifications and structural changes in LDL⁻

LC/MS/MS (Table 1) and circular dichroism (Fig. 2) analyses indicated apoB-100 protein modifications and conformational changes inherent in LDL⁻. Although there were no observed nitrated peptides by LC/MS/MS in native- and total-LDL fractions *in vivo*, there was nitration that was quantified by LC/EIS/MS analysis. The amount of nitration observed for native LDL was 100-fold lower than LDL⁻ and tLDL was approximately 10- to 12-fold lower. These findings further support the notion that the LDL-particle is the modified LDL subfraction *in vivo* as well as may support the LDL⁻ hypothesis. Tyrosine nitration in LDL⁻ (Table 1) in α_1, α_2, and α_3 helices as well as β_2 sheets as well as cysteine oxidation in β_1 to cysteic acid (Fig. 12) seem to assist the loss of α-helical structure in

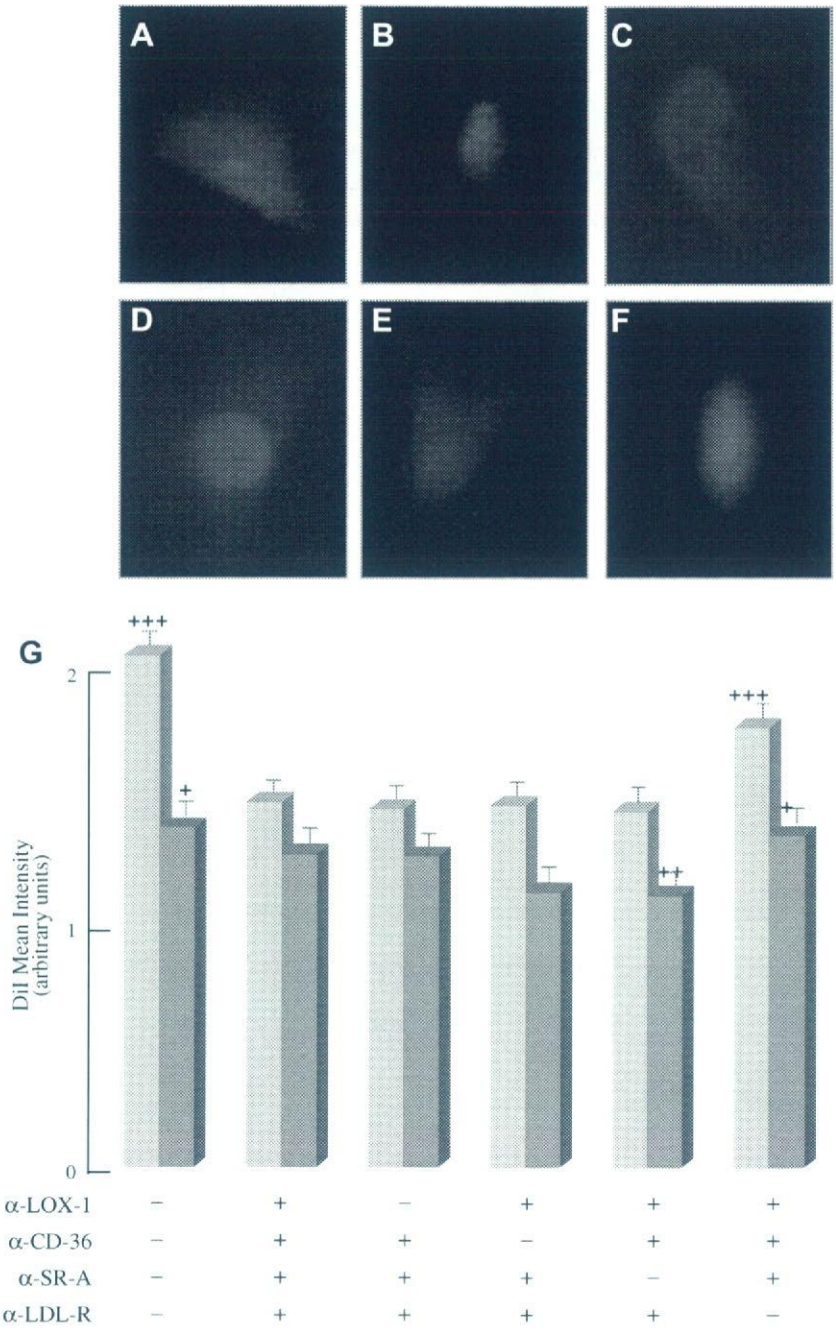

Fig. 10. Uptake of control-LDL after receptor blocking. LDL receptor blocking was performed for 1 h at 37 °C and uptake was determined at 37 °C with 10 μg/ml Dil-control-LDL and 10 μg/ml Dil-control-LDL with 200 μg/ml excess unlabeled LDL for 4 h by the following conditions; (A) no receptor blocking with 10 μg/ml Dil-control-LDL, (B) all four receptor's blocked with 10 μg/ml Dil-control-LDL (C) active LOX-1, (D) active CD36 with 10 μg/ml Dil-control-LDL, (E) active SR-A with 10 μg/ml Dil-control-LDL, and (F) active LDL-R with 10 μg/ml Dil-control-LDL. Uptake mean intensity of Dil-control-LDL was quantified using Axiom 200 M Zeiss Fluorescent Microscope (G). Images are not shown for excess unlabeled control-LDL but intensities were quantified. Experiments were performed in triplicate and statistical significance was determined to all receptors blocked to determine receptors significantly involved in the uptake of Dil-labeled control-LDL ($n = 3$, $^{*}P < 0.05$, $^{**}P < 0.01$, $^{***}P < 0.001$). ▒ – 10 mg/ml Dil-labeled control-LDL, ■ – 10 mg/ml Dil-labeled control-LDL + 200 mg/ml excess unlabeled control-LDL.

LDL^{-} and increase β-turn, parallel- and anti-parallel sheets, and random coil structures (Fig. 2). Of note, nitration of apoB-100 occurs in the α-helical structures containing the highest percentage of tyrosine per total amino acid residues: α_1 appears to be more susceptible to nitrotyrosine formation, whereas β_1 seemed resistant to nitration and susceptible to cysteine oxidation. Nitration of α-helices appears to contribute to protein unfolding, whereas the oxidation of one of the nine free cysteines (in β_1 sheets) may be involved in the increased electronegativity of the particle.

A functional role for ONOO^{-} in LDL^{-} formation

Treatment of native LDL with either ONOO^{-} (Fig. 3) or SIN-1 (Fig. 5) resulted in extensive tyrosine nitration (Table 2; Fig. 12), accumulation of lipid peroxides, and loss of α-helical structure (Fig. 4) and, as a corollary, formation of LDL^{-} Figs. 3D, 5D). It may be surmised, hence, that nitrotyrosine- and lipid peroxide accumulation are synergistically responsible for unfolding of α-helices inherent in LDL^{-} formation.

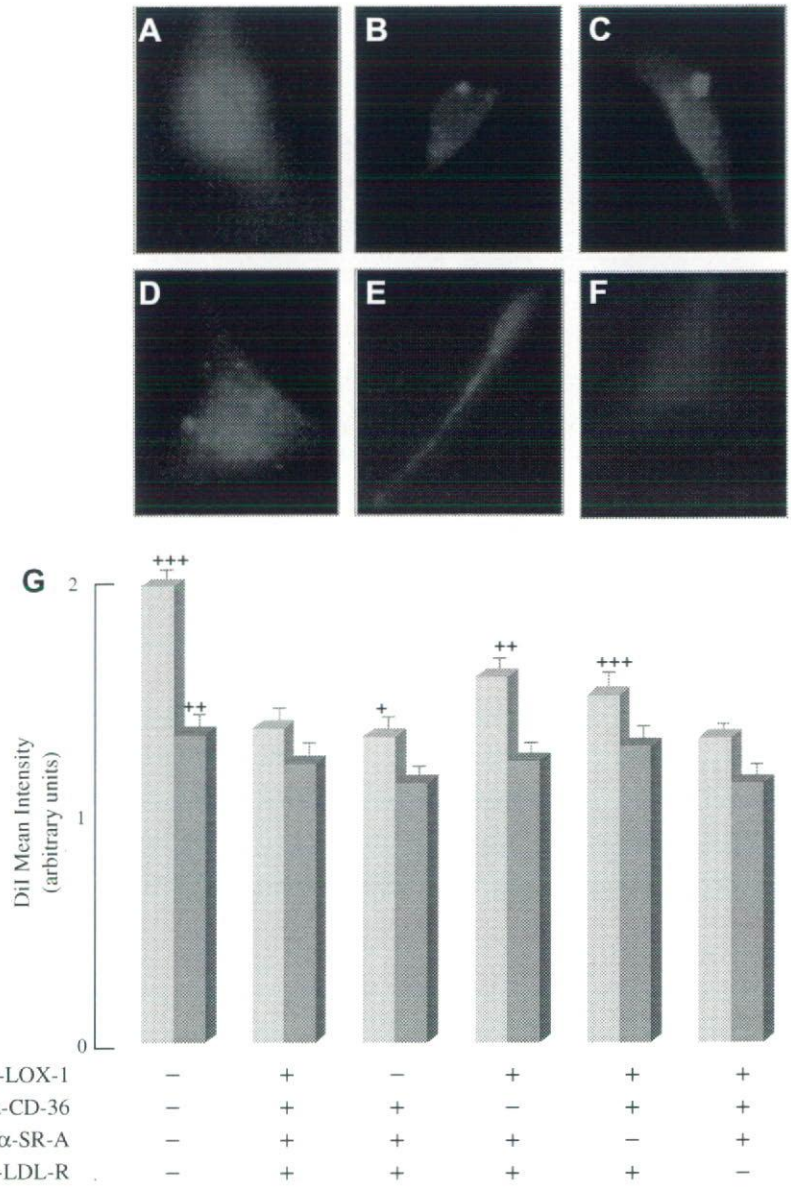

Fig. 11. Uptake of $ONOO^-$-LDL after receptor blocking. LDL receptor blocking was performed for 1 h at 37 °C and uptake was determined at 0 °C with 10 μg/ml Dil-$ONOO^-$-LDL and 10 μg/ml Dil-$ONOO^-$-treated LDL with 200 μg/ml excess unlabeled $ONOO^-$-treated LDL for 4 h by the following conditions; (A) no receptor blocking with 10 μg/ml Dil-$ONOO^-$-treated LDL, (B) all four receptor's blocked with 10 μg/ml Dil-$ONOO^-$-treated LDL (C) active LOX-1, (D) active CD36 with 10 μg/ml Dil-$ONOO^-$-treated LDL, (E) active SR-A with 10 μg/ml Dil-$ONOO^-$-treated LDL, and (F) active LDL-R with 10 μg/ml Dil- $ONOO^-$-treated LDL. Binding mean intensity of Dil-$ONOO^-$-treated LDL was quantified using Axiom 200 M Zeiss Fluorescent Microscope (G). Images are not shown for excess unlabeled $ONOO^-$-treated LDL but intensities were quantified. Experiments were performed in triplicate and statistical significance was determined to all receptors blocked to determine receptors significantly involved in the binding of Dil-labeled $ONOO^-$-treated LDL. Experiments were performed in triplicate and statistical significance was determined to all receptors blocked ($n = 3$, $^*P < 0.05$, $^{**}P < 0.01$, $^{***}P < 0.001$). ▒ – 10 mg/ml Dil-labeled $ONOO^-$-treated LDL, ■ – 10 mg/ml Dil-labeled $ONOO^-$-treated LDL + 200 mg/ml excess unlabeled $ONOO^-$-treated LDL.

Specific cellular receptors for LDL^-

The aforementioned protein modifications and structural changes in LDL^- may suggest an LDL receptor (LDL-R)-independent mechanism for binding and uptake of LDL^- to and into BAEC cells; this notion is supported by the following (a) LDL nitration coincides with the binding sites to LDL-R (encompassing amino acid residues 3359 and 3369 in β_2) and (b) there is evidence that $ONOO^-$-treated LDL binds to CD36 [35]. These findings are further confirmed by the binding and uptake of $ONOO^-$-treated LDL to LOX-1, CD36, and SR-A receptors in BAEC with minimal involvement of the non-atherogenic LDL-R. It is worth noting that most uptake and binding in control-LDL was dependent on LDL-R and independent of oxLDL-R suggesting the non-atherogenic properties of control-LDL. However, there was still a minimal binding and uptake to LOX-1, CD36, and SR-A in control-LDL suggesting the importance of *in vivo* modified LDL^-. It was also evident that $ONOO^-$-treated LDL did not induce LDL-R mediated uptake suggesting that it is not being endocytosed through an aggregated-LDL uptake mechanism. The *in vivo* LDL^- nitration pattern and structure as well as $ONOO^-$-modified LDL demonstrate that $ONOO^-$ is the most likely mechanism of protein nitration *in vivo* and suggests that protein unfolded LDL induces scavenger receptor dependent binding and uptake and is further supported by enzymatic modifications that induce protein unfolding [3,17]. Nitrated LDL is also involved in an LDL-R independent binding and uptake med-

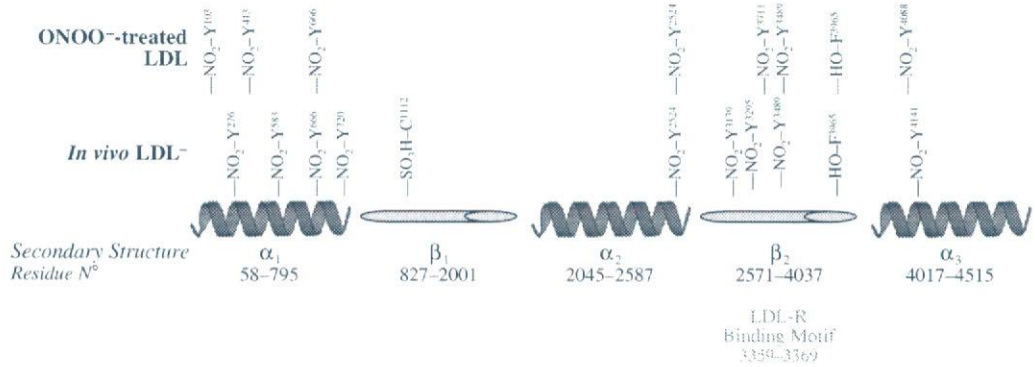

Fig. 12. Site of chemical modifications in *in vivo* LDL⁻ and ONOO⁻-treated LDL. The secondary structure of the apoB-100 is shown. The pentapartite structure however is not drawn to scale. Data from Tables 1 and 2 were used to assign the chemical modifications in LDL⁻ and ONOO⁻-treated LDL.

iated by SR-A, LOX-1, and CD36, thus strengthening the pathophysiological significance of ONOO⁻-driven LDL modifications, its unfolding, and the pathogenesis of atherosclerosis.

Tyrosine nitration and lipid peroxidation appear to disturb the phospholipid belt of LDL and hydrophobic stacking of aromatic amino acids in the lipid core. The three α-helices have the highest percentage of tyrosine residues; it may be hypothesized that nitration of these tyrosine residues would have a synergistic affect upon protein unfolding along with lipid peroxide formation. Addition of a nitro group to tyrosine involves the addition of a hydrophilic moiety with a net electrostatic charge (Zwitterion); aromatic groups are involved in hydrophobic stacking interactions in proteins as well as in protein-lipid bilayer interface. Therefore, nitration in α-helices is expected to interfere with hydrophobic stacking in the lipid core of the LDL particle and possibly with the phospholipid belts of α_2 and α_3 helices, leading to protein unfolding. Furthermore, peroxidation of lipids in LDL seem to cause unfolding of the apoB-100 protein [11]. The phospholipid belt in α_2 and α_3 is stabilized by electrostatic bonds between negatively charged phospho head groups and positively charged lysine/arginine residues. Peroxidation of long chain poly unsaturated fatty acyl chains of the phospholipid belts and the addition of molecular oxygen will increase the hydrophilicity of the fatty acyl chains of phospholipids, thus resulting in both the migration out of the lipid phase and an increasing surface area to volume ratio of the lipid core (increased hydrophilic surface). This increased strain would induce α_2 and α_3 to stretch and adopt a new confirmation. This mechanism strengthens the significance of the phospholipid belts (α_2 and α_3) in maintaining particle protein/lipid integrity, particle structure, proper electrostatic interactions, and aromatic stacking.

Regardless of its mechanism, these findings suggest that protein unfolding may be the main contributor to LDL⁻-induced atherosclerosis. The extensive nitration of apoB-100 in the α-helices and β-sheets of LDL⁻ and its absence in native LDL suggest that the latter is not or has not been subjected to nitrative stress *in vivo*. In response to phospholipase A_2 and oxidation *in vitro*, modifications of LDL render the formation of an electronegative sub-fraction with secondary structural changes similar to those of *in vivo* LDL⁻. As an emergent marker for coronary artery disease, nitrotyrosine is prominent in atherosclerotic lesions as well as LDL isolated from atherosclerotic lesions [5]. In this context, this study established similar apoB-100 protein nitration patterns and secondary protein structural changes in *in vivo* circulating LDL⁻ and ONOO⁻-treated LDL. Moreover, binding and uptake of the protein unfolded fraction (LDL⁻) was higher than that of native LDL and uptake of ONOO⁻-treated LDL is dependent on scavenger receptors LOX-1, CD36, and SR-A and is not on dependent on LDL-R whereas the control-LDL subfraction is dependent on anti-atherogenic LDL-R and not dependent on atherogenic LOX-1, CD36, and SR-A scavenger receptors in BAEC.

Acknowledgments

We thank Dr. Ralf Langen and team for support with CD spectra analyses and CD spectrophotometer. We also thank Staley L. Hazen and team for their analysis of nitrotyrosine in ONOO⁻-treated LDL by LC/EIS/MS. This work was supported by AHA GIA 0655051Y (TKH), NIH HL 83015 (TKH), and HL NIH HL068689 (TKH). The authors express gratitude to Dr. Alex Sevanian.

Appendix A. Supplementary data

Supplementary data associated with this article can be found, in the online version, at doi:10.1016/j.abb.2008.07.026.

References

[1] A. Colell, C. Garcia-Ruiz, J.M. Lluis, O. Coll, M. Mari, J.C. Fernandez-Checa, J. Biol. Chem. 278 (2003) 33928–33935.
[2] T. Hevonoja, M.O. Pentikainen, M.T. Hyvonen, P.T. Kovanen, M. Ala-Korpela, Biochim. Biophys. Acta 1488 (2000) 189–210.
[3] L. Asatryan, R.T. Hamilton, J.M. Isas, J. Hwang, R. Kayed, A. Sevanian, J. Lipid Res. 46 (2005) 115–122.
[4] M. Torzewski, K.J. Lackner, Clin. Chem. Lab. Med. 44 (2006) 1389–1394.
[5] C. Leeuwenburgh, M.M. Hardy, S.L. Hazen, P. Wagner, S. Oh-ishi, U.P. Steinbrecher, J.W. Heinecke, J. Biol. Chem. 272 (1997) 1433–1436.
[6] E. Koller, I. Volf, A. Gurvitz, F. Koller, Pathophysiol. Haemost. Thromb. 35 (2006) 322–345.
[7] E. Malle, G. Marsche, J. Arnhold, M.J. Davies, Biochim. Biophys. Acta 1761 (2006) 392–415.
[8] B. Osterud, E. Bjorklid, Physiol. Rev. 83 (2003) 1069–1112.
[9] L.F. Gomes, A.F. Alves, A. Sevanian, A. Peres Cde, M.S. Cendoroglo, C. de Mello-Almada, L.M. Quirino, L.R. Ramos, V.B. Junqueira, Antioxid. Redox Signal. 6 (2004) 237–244.
[10] J. Hwang, M. Rouhanizadeh, R.T. Hamilton, T.C. Lin, J.P. Eiserich, H.N. Hodis, T.K. Hsiai, Free Radic. Biol. Med. 41 (2006) 568–578.
[11] F. Ursini, K.J. Davies, M. Maiorino, T. Parasassi, A. Sevanian, Trends Mol. Med. 8 (2002) 370–374.
[12] S.R. Thomas, M.J. Davies, R. Stocker, Chem. Res. Toxicol. 11 (1998) 484–494.
[13] H. Botti, C. Batthyany, A. Trostchansky, R. Radi, B.A. Freeman, H. Rubbo, Free Radic. Biol. Med. 36 (2004) 152–162.
[14] S.L. Hazen, J.R. Crowley, D.M. Mueller, J.W. Heinecke, Free Radic. Biol. Med. 23 (1997) 909–916.
[15] T.K. Hsiai, J. Hwang, M.L. Barr, A. Correa, R. Hamilton, M. Alavi, M. Rouhanizadeh, E. Cadenas, S.L. Hazen, Free Radic. Biol. Med. 42 (2007) 519–529.
[16] S.R. Han, A. Momeni, K. Strach, P. Suriyaphol, D. Fenske, K. Paprotka, S.I. Hashimoto, M. Torzewski, S. Bhadki, M. Husmann, Atheroscler. Thromb. Vasc. Biol. 23 (2003) 661–667.
[17] K. Dersch, H. Ichijo, S. Bhakdi, M. Husmann, Cell Death Differ. 12 (2005) 1107–1114.
[18] M. Torzewski, P. Suriyaphol, K. Paprotka, L. Spath, V. Ochsenhirt, A. Schmitt, S.R. Han, M. Husman, V.B. Gerl, S. Bhakdi, K.J. Lackner, Atheroscler. Thromb. Vasc. Biol. 24 (2004) 2130–2136.

[19] A.F. Saad, G. Virella, C. Chassereau, R.J. Boackle, M.F. Lopes-Virella, J. Lipid Res. 47 (2006) 1975–1983.
[20] T.K. Hsiai, S.K. Cho, P.K. Wong, M. Ing, A. Salazar, A. Sevanian, M. Navab, L.L. Demer, C.M. Ho, FASEB J. 17 (2003) 1648–1657.
[21] K. Jagavelu, U.J. Tietge, M. Gastel, H. Drexler, B. Schieffer, U. Bavendiek, Circ. Res. 101 (2007) 1104–1112.
[22] L. Zheng, B. Nukuna, M.L. Brennan, M. Sun, M. Goormastic, M. Settle, D. Schmitt, X. Fu, L. Thomson, P.L. Fox, H. Ischiropoulos, J.D. Smith, M. Kinter, S.L. Hazen, J. Clin. Invest. 114 (2004) 529–541.
[23] B. Ferraro, F. Galli, B. Frei, E. Kingdon, F. Canestrari, C. Rice-Evans, U. Buoncristiani, A. Davenport, K.P. Moore, Kidney Int. 63 (2003) 2207–2213.
[24] Y. Yamaguchi, S. Matsuno, S. Kagota, J. Haginaka, M. Kunitomo, Atherosclerosis 172 (2004) 259–265.
[25] M. Spite, S.P. Baba, Y. YAhmed, O.A. Barski, K. Nijhawan, J.M. Petrash, A. Bahatnagar, S. Srivastava, Biochem. J. 405 (2007) 95–105.
[26] J. Hwang, J. Wang, P. Morazzoni, H.N. Hodis, A. Sevanian, Free Radic. Biol. Med. 34 (2003) 1271–1282.
[27] R. Stocker, J.F. Keaney Jr., J. Thromb. Haemost. 3 (2005) 1825–1834.
[28] D. Behr-Roussel, A. Rupin, S. Simonet, E. Bonhomme, S. Coumailleau, A. Cordi, B. Serkiz, J.N. Fabiani, T.J. Verbeuren, Circulation 102 (2000) 1033–1038.
[29] H.N. Hodis, D.M. Kramsch, P. Avogaro, G. Bittolo-Bon, G. Cazzolato, J. Hwang, H. Peterson, A. Sevanian, J. Lipid Res. 35 (1994) 669–677.
[30] M. Feelisch, J. Ostrowski, E. Noack, J. Cardiovasc. Pharmacol. 14 (Suppl. 11) (1989) S13–S22.
[31] A. Ducret, I. Van Oostveen, J.E. Eng, J.R. Yates III, R. Aebersold, Protein Sci. 7 (1998) 706–719.
[32] D.N. Perkins, D.J.C. Pappin, D.M. Creasy, J.S. Cottrell, Electrophoresis 20 (1999) 3551–3567.
[33] R. Ricci, G. Sumara, I. Sumara, I. Rozenberg, M. Kurrer, A. Akhmedov, M. Hersberger, U. Eriksson, F.R. Eberli, B. Becher, J. Boren, M. Chen, M.I. Cybulsky, K.J. Moore, M.W. Freeman, E.F. Wagner, C.M. Matter, T.F. Luscher, Science 306 (2004) 1558–1561.
[34] A. Sevanian, G. Bittolo-Bon, G. Cazzolato, H. Hodis, J. Hwang, A. Zamburlini, M. Maiorino, F. Ursini, J. Lipid Res. 38 (1997) 419–428.
[35] R.A. Guy, G.F. Maguire, I. Crandall, P.W. Connelly, K.C. Kain, Atherosclerosis 155 (2001) 19–28.

Papers in Press. Published December 12, 2008 as doi:10.1373/clinchem.2008.119750
The latest version is at http://www.clinchem.org/cgi/doi/10.1373/clinchem.2008.119750

Clinical Chemistry 55:2
000–000 (2009)

Oxidized LDL Receptor LOX-1 Binds to C-reactive Protein and Mediates its Vascular Effects

Yoshiko Fujita,[1] Akemi Kakino,[1] Norihisa Nishimichi,[2] Saburo Yamaguchi,[1] Yuko Sato,[1] Sachiko Machida,[3] Luciano Cominacini,[4] Yves Delneste,[5,6] Haruo Matsuda,[2] and Tatsuya Sawamura[1*]

BACKGROUND: C-reactive protein (CRP) exerts biological activity on vascular endothelial cells. This activity may promote atherothrombosis, but the effects of this activity are still controversial. Lectin-like oxidized LDL receptor-1 (LOX-1), the oxidized LDL receptor on endothelial cells, is involved in endothelial dysfunction induced by oxidized LDL.

METHODS: We used laser confocal microscopy to examine and fluorescence cell image analysis to quantify the binding of fluorescently labeled CRP to cells expressing LOX-1. We then examined the binding of unlabeled CRP to recombinant human LOX-1 in a cell-free system. Small interfering RNAs (siRNAs) against LOX-1 were applied to cultured bovine endothelial cells to analyze the role of LOX-1 in native cells. To observe its in vivo effects, we injected CRP intradermally in stroke-prone spontaneously hypertensive (SHR-SP) rats and analyzed vascular permeability.

RESULTS: CRP bound to LOX-1–expressing cells in parallel with the induction of LOX-1 expression. CRP dose-dependently bound to the cell line and recombinant LOX-1, with significant binding detected at 0.3 mg/L CRP concentration. The K_d value of the binding was calculated to be 1.6×10^{-7} mol/L. siRNA against LOX-1 significantly inhibited the binding of fluorescently labeled CRP to the endothelial cells, whereas control RNA did not. In vivo, intradermal injection of CRP-induced vascular exudation of Evans blue dye in SHR-SP rats, in which expression of LOX-1 is greatly enhanced. Anti–LOX-1 antibody significantly suppressed vascular permeability.

CONCLUSIONS: CRP and oxidized LDL-receptor LOX-1 directly interact with each other. Two risk factors for ischemic heart diseases, CRP and oxidized LDL, share a common molecule, LOX-1, as their receptor.

C-reactive protein (CRP)[7] is an acute-phase plasma protein that is synthesized by hepatocytes in response to inflammation and tissue damage; the latter can cause a 1000-fold or more increase in the human plasma concentrations of high-sensitivity CRP (hsCRP). For this reason hsCRP has long been used as an inflammatory biomarker *(1)*. CRP recognizes phosphocholine *(2)* and other various ligands, including phosphoethanolamine, chromatin, histones, fibronectin, and oxidized LDL *(3, 4)*. Recent epidemiological studies have shown that even the slightest increase in serum concentration of hsCRP can be a major risk indicator for ischemic heart disease *(5–7)*. Activation of the classical complement pathway through direct interaction with C1q is an established function of CRP. It is reported that administration of human CRP in a rat model of myocardial infarction activates complement systems, leading to increases in the size of myocardial infarction *(8)*, and that the chemical blockade of CRP prevents these deleterious effects and suppresses the myocardial infarction *(9)*. In addition, a number of recent reports have shown that CRP induces endothelial activation/dysfunction leading to atherothrombosis *(10)*. Because the earliest CRP reports may have reflected the effects of contaminants such as bacterial lipopolysaccharide and azide rather than CRP, there have been subsequent heated debates concerning CRP functions and actions

[1] Department of Vascular Physiology, National Cardiovascular Center Research Institute, Suita, Osaka, Japan; [2] Laboratory of Immunobiology, Department of Molecular and Applied Biosciences, Graduate School of Biosphere Science, Hiroshima University, Hiroshima, Japan; [3] National Food Research Institute, Tsukuba, Japan; [4] Department of Biomedical and Surgical Sciences, University of Verona, Verona, Italy; [5] INSERM, U564, University of Angers, Angers, France; [6] Immunology and Allergology Laboratory, University Hospital of Angers, Angers, France
* Address correspondence to this author at: Department of Vascular Physiology, National Cardiovascular Center Research Institute, 5-7-1 Fujishirodai, Suita, Osaka 565-8565, Japan. Fax +81-6-6835-5329; e-mail t-sawamura@umin.ac.jp.
Received October 27, 2008; accepted November 18, 2008.
Previously published online at DOI: 10.1373/clinchem.2008.119750
[7] Nonstandard abbreviations: CRP, C-reactive protein; hsCRP, high-sensitivity CRP; LOX-1, lectin-like oxidized LDL receptor-1; siRNA, small interfering RNA; BAEC, bovine aortic endothelial cells; WKY, Wistar Kyoto; SHR-SP, stroke-prone spontaneously hypertensive.

(11, 12). CRP preparations free from lipopolysaccharide and azide, however, reportedly have shown significant effects on endothelial activation. Fcγ receptors are postulated to be the receptors that mediate the effects of CRP outside of complement activation *(12–14)*.

Lectin-like oxidized LDL receptor 1 (LOX-1) was originally found and identified as an endothelial receptor for oxidized LDL *(15)*. Activation of LOX-1 in endothelial cells induces the generation of superoxide, a reduction in the release of nitric oxide, and the expression of proatherogenic molecules such as endothelin-1, monocyte chemoattractant protein 1, vascular cell adhesion molecule 1, and intercellular adhesion molecule 1*(16–18)*. The overexpression of LOX-1 in mice enhances oxidative stress and the expression of adhesion molecules in blood vessels, accelerating atheroma-like lipid deposition in intramyocardial vessels *(19)*. Deletion of LOX-1 in mice preserves endothelial function, leading to reduction in atherogenesis *(20)*. In addition to oxidized LDL, LOX-1 binds various ligands, e.g., apoptotic cells, activated platelets, leukocytes, and bacteria *(21–25)*. Related functions of LOX-1 include involvement in inflammation, myocardial infarction, and intimal thickening after balloon catheter injury *(23, 26–29)*.

Because the changes induced by CRP and by LOX-1 activation overlap, we investigated the physical interactions between CRP and LOX-1 that may be related to cardiovascular pathophysiology.

Materials and Methods

CRP

Human CRP purified from pleural fluid was purchased from Chemicon (AG723). Sodium azide in the solution was removed by dialysis performed 3 times against a 3000-fold volume of Dalbecco's PBS (Wako). Gram-negative bacterial endotoxins were undetectable by limulus amebocyte lysate (Associates of Cape Cod), which can detect as low as 30 endotoxin units/L of endotoxins. CRP preparations from 2 other distributers, one purified from human plasma (C4063, Sigma) and the other from human serum (#236603, Calbiochem), were also subjected to cell-free analyses.

FLUORESCENTLY LABELED CRP

CRP was fluorescently labeled with an Alexa Fluor 546 protein-labeling kit (Invitrogen) and dialyzed 3 times against a 3000-fold volume of PBS.

CELL LINE EXPRESSING HUMAN LOX-1 (HLOX-1-CHO) DRIVEN BY TETRACYCLINE-INDUCIBLE PROMOTER

cDNA encoding the human LOX-1 (Genbank NM002543) was subcloned into pTRE2hyg (Clonetech). CHO-K1 Tet-On cells (Clonetech) were transfected with pTRE2hyg-human LOX-1 by Lipofectamin-2000 transfection reagent (Invitrogen) according to the manufacture's instructions. The stable transformants were selected with 400 mg/L of hygromycin B (Wako). The resistant clones that express LOX-1 in response to doxycycline (Calbiochem) were selected for use in these experiments. The LOX-1 expression was induced with doxycyline at the indicated concentration in Ham's F-12 medium (Gibco)/10% fetal bovine serum 24 h before the experiments. Cells were washed twice with Ham's F-12/10 mmol/L HEPES and chilled on ice for 30 min. Then, the medium was replaced with the indicated concentration of Alexa 546-CRP–containing ice-cold Ham's F-12/10 mmol/L HEPES, and cells were incubated on ice for 1 h. After being washed with ice-cold PBS, the cells were fixed with phosphate-buffered formalin (Wako). The expression of LOX-1 was visualized by immunostaining with antihuman LOX-1 antibody (TS92) *(30)* combined with Alexa 488-anti-human IgG (1:2000) (Invitrogen). Then, the specimens were subjected to microscopic analysis with confocal laser microscope (TCS SP5, Leica), and quantitative fluorescence cell image analysis with the IN Cell analyzer 1000 system (GE Healthcare).

TRANSIENT GENE EXPRESSION ASSAY

COS7 cells maintained with DMEM/10% fetal bovine serum were seeded 1 day before transfection. The cells at 80%–90% confluency were transfected with indicated plasmid by use of Lipofectamin 2000 transfection reagent (Invitrogen). After 24 h, the cells were chilled on ice for 30 min and washed with ice-cold PBS. Then, the medium was replaced with the indicated concentration of Alexa 546-CRP–containing ice-cold DMEM/10 mmol/L HEPES, and cells were incubated on ice for 1 h. After being washed with ice-cold PBS, the cells were fixed with phosphate-buffered formalin (Wako). The expression of each receptor was assessed by immunostaining with anti-V5 antibody (1:1000) (Nacalai Tesque) combined with Alexa 488-antimouse IgG (1:2000) (Invitrogen). The nuclei of the cells were counterstained with 0.5 mg/L DAPI (Sigma). Quantitative analysis was performed with an IN Cell Analyzer.

RECOMBINANT LOX-1

cDNA encoding extracellular domain of human LOX-1 (61–273) was subcloned into pcDNA4 with a chicken IgG light chain leader peptide in the N-terminal and V5-6xHis tag in the C-terminus. The plasmid was transfected into FreeStyle 293-F cells (Invitrogen). After 4 days, the recombinant protein was purified from culture supernatant with Ni-NTA superflow (Qiagen) according to the manufacturer's instructions.

CRP-LOX-1 INTERACTION ASSAY BY ELISA

Recombinant human LOX-1 (0.1 μg) or BSA (0.1 μg, Sigma) was immobilized to each well of 384-well plates (Maxisorp, Nunc) by incubation overnight at 4 °C in PBS. After 2 washes with PBS, the plates were blocked with 80 μL of 20% ImmunoBolock (DS Pharma)/PBS at 4 °C for 8 h. After 2 washes with PBS, CRP in the reaction buffer (10 mmol/L HEPES, 150 mmol/L NaCl, 2 mmol/L $CaCl_2$, 1% BSA, pH 7.0) was added to each well, and incubated at 4 °C overnight. The plates were then washed 3 times with PBS and incubated for 2 h with horseradish peroxidase–conjugated antihuman CRP antibody (1:5000) (Bethyl) in PBS, 1% BSA. After 5 washes with PBS, peroxidase activity was determined with a TMB Peroxidase EIA Substrate kit (Bio-Rad). For the analyses of the binding of heat-denatured CRP, CRP solution in PBS was heated in boiling water for 5 min before use. The immunoreactivity of the denatured CRP to the anti-CRP antibody was examined by ELISA of immobilized CRP. The indicated amounts of CRP, denatured CRP, or BSA were immobilized, and blocking was performed as above. Then, the immobilized proteins were detected by the horseradish peroxidase–conjugated antihuman CRP antibody as above.

BIACORE ANALYSES

The K_d value of the CRP binding to LOX-1 was measured by surface plasmon resonance on a BIACORE 2000 (GE Healthcare). Recombinant LOX-1 was immobilized on a research-grade CM5 sensor chip (GE Healthcare) by use of an Amine coupling kit (GE Healthcare) according to the manufacturer's instructions. BSA was immobilized on a sensor chip by the same method described above, and used as reference. We then injected 30 μL of the analytes (CRP 0.45, 0.89, 1.78, and 3.56 μmol/L) in 10 mmol/L HEPES, 150 mmol/L NaCl, 2 mmol/L $CaCl_2$, 1% BSA (pH 7.0) at a flow rate of 20 μL/min for 120 s, and dissociation in the same buffer was monitored for 120 s. After each analysis, the sensor chip was regenerated with 5 μL of 50 mmol/L NaOH at a flow late of 60 μL/min. We calculated K_d values by using a 1:1 Langmuir binding model with BIAevaluation software version 3.0 (GE Healthcare).

RNA INTERFERENCE

We designed small interfering RNA (siRNA) duplex oligoribonucleotides targeting the bovine LOX-1 coding region (Genbank NM174132) by using the Block-iT RNAi (RNA interference) designer program from the Invitrogen website. The stealth RNAi negative control duplex (Invitrogen) was used as a negative control. The siRNA sequences are as follows: si1 for LOX-1 (204–228), 5′-UUCUUUAUGAGAUCAGAGACCUGGG-3′ and si2 for LOX-1 (396–420), 5′-ACUUCUUGGAGAUUCAGGUUCUGGC-3′.

Bovine aortic endothelial cells (BAEC) and bLOX-1-CHO (Chinese hamster ovary cells stably expressing bovine LOX-1) *(15)* were maintained with DMEM (Gibco)/10% fetal bovine serum/1% (vol/vol) Antibiotic-Antimycotic (Gibco) and Ham's F-12 medium/10% fetal bovine serum containing 10 mg/L blasticidin (Kaken Pharmaceutical), respectively. The cells were seeded 1 day before transfection. The following day, the cells at 50%–60% confluency were transfected with siRNA oligos or the control siRNA by use of Lipofectamin RNAiMAX tansfection reagent (Invitrogen) according to the manufacture's instructions. After incubation at 37 °C for 24 h, the effects of downregulation of expression of the LOX-1 gene [oxidized low density lipoprotein (lectin-like) receptor 1] were examined. Suppression of LOX-1 expression was confirmed by the immunostaining with anti–LOX-1 antibody (TS20) combined with Alexa488-antimouse IgG (1:2000) (Invitrogen) and quantitative analysis with the IN Cell analyzer. All transfections were performed in triplicate.

ANIMALS

All protocols were approved by the Institutional Animal Care and Use Committee of the National Cardiovascular Center. Male Wistar Kyoto (WKY) rats and stroke-prone spontaneously hypertensive (SHR-SP) rats (SLC) were used at 8 weeks of age for experiments.

IMMUNOHISTOCHEMICAL ANALYSIS

For the analysis by confocal laser microscope, rat dermal tissue was snap-frozen in liquid nitrogen and sectioned at 10 μm with a cryostat (Leica). The sections were fixed by 4% formaldehyde for 15 min, blocked with 20% Blockace (Snow brand) for 1 h at room temperature, and then stained with 2 mg/L Alexa633 anti–LOX-1 antibody (TS20) or 0.2 mg/L R-phycoeythrin–conjugated anti-rat CD31 antibody (TLD-3A12, BD). Labeling of the anti–LOX-1 antibody was performed with an Alexa Fluor 633 protein-labeling kit (Invitrogen) according to the manufacturer's instructions.

FLUORESCENT MILES PERMEABILITY ASSAY

The rats were anesthetized with Nembutal (50 mg/kg body weight, administered intraperitoneally), and warmed on the thermal control plate set at 37 °C (HI1220, Leica). Hairs in the dorsal skin region were shaved for fluorescence analyses. CRP, BSA, or vascular endothelial growth factor (Sigma) dissolved in 10 μL of PBS were intradermally injected to the shaved lumbar area of dorsal skin. In some experiments, anti–LOX-1 antibody (TS20, 3 μg) *(22)* or nonimmune mouse IgG (3 μg, Sigma) was coinjected with CRP. Thirty

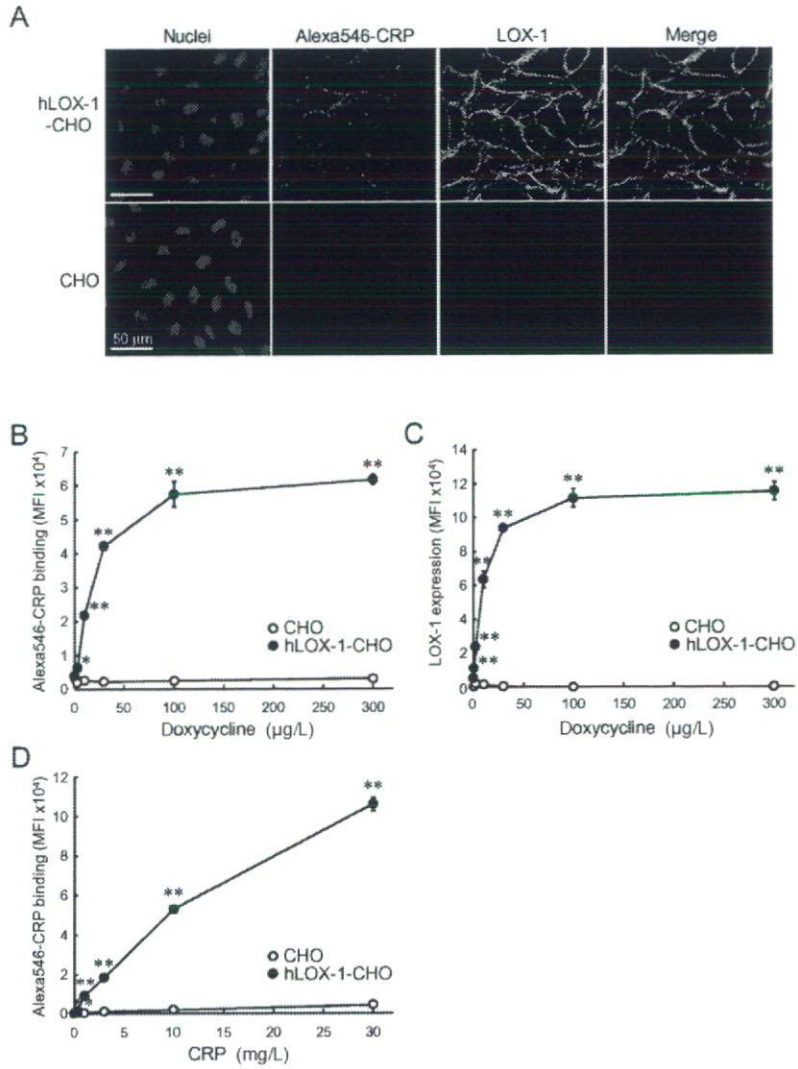

Fig. 1. Fluorescently labeled CRP binds to LOX-1.

(A) Analysis of hLOX-1-CHO (Chinese hamster ovary cell expressing human LOX-1 driven by tetracycline-inducible promoter) (*upper panels*) and control CHO cells (*lower panels*) stained with anti–LOX-1 antibody (*green*) or incubated with Alexa546-CRP (10 mg/L, *red*) by laser confocal microscopy. The nuclei of the cells were counterstained with DAPI (*blue*). The merged image of Alexa546-CRP and LOX-1 indicates colocalization of these molecules on the cell surface. (B, C) Alexa546-CRP (10 mg/L) binding (B) to hLOX-1-CHO in response to the induction of the expression of LOX-1 (C) by increasing dose of doxycycline (0–300 mg/L). (D) Dose-dependent binding of Alexa546-CRP (0–30 mg/L) to hLOX-1-CHO that were pretreated with 100 μg/L of doxycycline. hLOX-1-CHO or control CHO cells were pretreated with indicated concentration of doxycycline to induce the expression of human LOX-1. Then, cells were incubated with Alexa546-CRP for 1h at 4 °C. The binding of Alexa546-CRP and the expression of the introduced protein were analyzed by IN Cell analyzer. The asterisks indicate significant difference vs CHO (*$P < 0.05$, **$P < 0.01$). MFI, mean fluorescence intensity.

minutes later, 2% Evans blue (Wako) in saline (Otsuka Pharma) was injected via the tail vein at a dose of 20 mg/kg weight of the rats. Vascular permeability was assessed by the exudation of Evans blue into the animal dorsal skin, detected with the Maestro Imaging System (CRi). A bandpass filter from 575–605 nm was used for excitation, and the fluorescence intensity at 680 nm was measured for quantitative analysis. The fluores-